NAVAL POSTGRADUATE SCHOOL

MONTEREY, CALIFORNIA

THESIS

STUDY OF THE PROGRESSIVE FAILURE OF COMPOSITES UNDER AXIAL LOADING WITH VARYING STRAIN RATES

by

Yew Khuan Boey

December 2011

Thesis Advisor:	Young Kwon
Second Reader:	Jarema Didoszak

Approved for public release; distribution is unlimited

THIS PAGE INTENTIONALLY LEFT BLANK

REPORT DOCUMENTATION PAGE			Form Approved OMB No. 0704–0188
Public reporting burden for this collection of information is estimated to average 1 hour per response, including the time for reviewing instruction, searching existing data sources, gathering and maintaining the data needed, and completing and reviewing the collection of information. Send comments regarding this burden estimate or any other aspect of this collection of information, including suggestions for reducing this burden, to Washington headquarters Services, Directorate for Information Operations and Reports, 1215 Jefferson Davis Highway, Suite 1204, Arlington, VA 22202–4302, and to the Office of Management and Budget, Paperwork Reduction Project (0704–0188) Washington DC 20503.			
1. AGENCY USE ONLY *(Leave blank)*	**2. REPORT DATE** December 2011	**3. REPORT TYPE AND DATES COVERED** Master's Thesis	
4. TITLE AND SUBTITLE Study of the Progressive Failure of Composites under Axial Loading with Varying Strain Rates		**5. FUNDING NUMBERS**	
6. AUTHOR(S) Yew Khuan Boey			
7. PERFORMING ORGANIZATION NAME(S) AND ADDRESS(ES) Naval Postgraduate School Monterey, CA 93943–5000		**8. PERFORMING ORGANIZATION REPORT NUMBER**	
9. SPONSORING /MONITORING AGENCY NAME(S) AND ADDRESS(ES) N/A		**10. SPONSORING/MONITORING AGENCY REPORT NUMBER**	
11. SUPPLEMENTARY NOTES The views expressed in this thesis are those of the author and do not reflect the official policy or position of the Department of Defense or the U.S. Government. IRB Protocol number _____N/A_____.			
12a. DISTRIBUTION / AVAILABILITY STATEMENT Approved for public release; distribution is unlimited		**12b. DISTRIBUTION CODE**	

13. ABSTRACT (maximum 200 words)

This study investigated the progressive damage/failure of composite panels with open circular holes under progressive axial loading. A series of experiments was carried out to determine the failure in laminated specimens with and without circular holes under tensile and compressive loads, respectively.

Different strain rate loading was applied to observe the rate effect on the damage initiation and propagation. Both uniform and non-uniform strain rate loads were applied to the composite specimens in order to understand the varying strain rate effect on the damage initiation and growth. With an increasing load, matrix cracking, surrounded by delamination occurred and lead to fiber breaking at the edge of the hole of high stress/strain concentration. When damage reached a critical state, the laminate failed catastrophically. By utilizing the optical microscope, the matrix cracking and fiber breaking leading to fracture was observed.

The fracture strength and strain of composites were varied depending on the applied strain rate loading. When the strain rate was changed halfway from the first rate to the second rate, the failure strength was relatively close to that at the constant second strain rate. However, fracture strain did not match with that of the second strain rate. Finally, the experimental results from the open hole tension was compared against Whitney-Nuiser Failure Prediction Theory, namely the Point Stress Criterion and Average Stress Criterion.

14. SUBJECT TERMS Compression test, tension test, varying strain effect, fracture strength, composite			**15. NUMBER OF PAGES** 79
			16. PRICE CODE
17. SECURITY CLASSIFICATION OF REPORT Unclassified	**18. SECURITY CLASSIFICATION OF THIS PAGE** Unclassified	**19. SECURITY CLASSIFICATION OF ABSTRACT** Unclassified	**20. LIMITATION OF ABSTRACT** UU

NSN 7540–01–280–5500 Standard Form 298 (Rev. 2–89)
Prescribed by ANSI Std. 239–18

THIS PAGE INTENTIONALLY LEFT BLANK

Approved for public release; distribution is unlimited

STUDY OF THE PROGRESSIVE FAILURE OF COMPOSITES UNDER AXIAL LOADING WITH VARYING STRAIN RATES

Yew Khuan Boey
B.Tech, National University of Singapore, 2009

Submitted in partial fulfillment of the
requirements for the degree of

MASTER OF SCIENCE IN MECHANICAL ENGINEERING

from the

NAVAL POSTGRADUATE SCHOOL
December 2011

Author: Yew Khuan Boey

Approved by: Young Kwon
Thesis Advisor

Jarema Didoszak
Second Reader

Knox Millsaps
Chair, Department of Mechanical and Aerospace Engineering

THIS PAGE INTENTIONALLY LEFT BLANK

ABSTRACT

This study investigated the progressive damage/failure of composite panels with open circular holes under progressive axial loading. A series of experiments was carried out to determine the failure in laminated specimens with and without circular holes under tensile and compressive loads, respectively.

Different strain rate loading was applied to observe the rate effect on the damage initiation and propagation. Both uniform and non-uniform strain rate loads were applied to the composite specimens in order to understand the varying strain rate effect on the damage initiation and growth. With an increasing load, matrix cracking, surrounded by delamination occurred and lead to fiber breaking at the edge of the hole of high stress/strain concentration. When damage reached a critical state, the laminate failed catastrophically. By utilizing the optical microscope, the matrix cracking and fiber breaking leading to fracture was observed.

The fracture strength and strain of composites were varied depending on the applied strain rate loading. When the strain rate was changed halfway from the first rate to the second rate, the failure strength was relatively close to that at the constant second strain rate. However, fracture strain did not match with that of the second strain rate. Finally, the experimental results from the open hole tension was compared against Whitney-Nuiser Failure Prediction Theory, namely the Point Stress Criterion and Average Stress Criterion.

THIS PAGE INTENTIONALLY LEFT BLANK

TABLE OF CONTENTS

LIST OF FIGURES

LIST OF TABLES

THIS PAGE INTENTIONALLY LEFT BLANK

LIST OF ACRONYMS AND ABBREVIATIONS

a	Crack or Notch half length; WEK critical damage length parameter; Bi-linear Cohesive Zone breakpoint (m)
a_0	Whitney-Nuismer Average Stress Criterion critical damage length parameter (m)
d_0	Whitney-Nuismer Point Stress Criterion critical damage length parameter (m)
CZM	Cohesive Zone Model
E	Modulus of Elasticity (Pa)
G	Modulus of Rigidity (Pa)
G_c	Fracture Energy (J/m^2)
G_I	Mode I energy release rate ($Pa\sqrt{m}$)
K_I	Mode I stress intensity factor
K_{IC}	Mode I critical stress intensity factor
K_t^{∞}	Stress Concentration Factor for an infinite plate
L	Length (m)
LEFM	Linear Elastic Fracture Mechanics
P	Load (N)
R,r	Notch or crack radius (m)
S	Applied remote stress (Pa)
v	Crack opening (m)
v_f	Critical crack opening (m)
W	Width (m)
WEK	Waddoups, Eisenmann, and Kaminski failure theory

x	Coordinate measured from center of notch perpendicular to direction of applied load (m)
X_C	Ultimate Compressive Strength (Pa)
X_T	Ultimate Tensile Strength (Pa)
υ	Poisson's ratio
ξ_1	R/(R+ d_0) in WNPS failure theory
ξ_2	R/(R+ a_0) in WNAS failure theory
σ	Applied Axial Stress (Pa)
σ_N	Notched tensile strength of a finite width plate (Pa)
σ_o	Unnotched tensile strength (Pa)
σ_y	Local stress component in the y-direction (Pa)

ACKNOWLEDGMENTS

I will like to thank Professor Young Kwon for his guidance throughout the course of this thesis study. Additionally, this thesis would not be possible without Professor Jarema Didoszak. I am very thankful to Dr. Chanman Park for explaining the testing equipment and procedures, and also assisting in the testing and setup phase. I am also very grateful to Mr. John Mobley for assistance in machining my specimens. I will also like to express my gratitude to LCDR Michael Violette who demonstrated the procedures for composite fabrication.

Finally, I will like to thank my wife, Lee Sin, for her understanding and support throughout my studies.

THIS PAGE INTENTIONALLY LEFT BLANK

I. INTRODUCTION

A. BACKGROUND

There has been increasing demand for lighter and stronger aircraft, missile and naval structures, which upsurges the interest in composite materials and research in this areas to fully exploit the composite properties. In order to fully exploit the composite properties, it is important to understand its characteristics and behavior under different loading. Thus, deformation and fracture behavior of fiber reinforced composites have received considerable attention because of their importance in structural applications and design. Designing the structural members requires open holes for connection, joint and access. These holes tend to cause stress concentration in areas adjacent to the hole's boundary, and they reduce the tensile and compressive load-bearing capacities of the member. Therefore, it is important to take note of this notch sensitivity when designing for bolt holes, joints or cut-out.

B. LITERATURE REVIEW

1. Experimental Test on Composites

There are many experimental tests performed on composites to understand the relationship between the strain rate and the composite's mechanical properties.

Norihiko Taniguchi [1] investigated the strain rate effects on tensile properties of composites loaded in the matrix-dominant direction, and the experimental results showed that the tensile strength of the composite increases linearly with the strain rate as the fiber orientation angles become higher. Although the Young's modulus and tensile strength increased with the strain rate in both the thermosetting and thermoplastic epoxy resin specimens, the strain rate effects of their tensile strength are quite minimal. Unlike the above properties, the Poisson's ratio decreases with the strain rate.

Comprehensive tensile tests were performed by Okoli and Smith [2] to examine a glass epoxy laminate at different rates of strain to determine the effects of strain rate on the Poisson's ratio of the material. The strain rate effects of most unfilled polymers can

be described by the Eyring theory of viscosity which assumes that the deformation of a polymer involves the motion of a chain molecule over potential energy barriers. The Eyring model suggests that yield strength varies linearly with the logarithm of the strain rate. The findings from the tensile tests suggest that Poisson's ratio is insensitive to strain rate. The presence of the fibers in the composite resulted in the lack of rate sensitivity in Poisson's ratio of the laminates.

Shokrieh and Omidi [3] studied the behavior of unidirectional glass fiber reinforced polymeric composites under uni-axial loading at quasi-static and intermediate strain rates of 0.001–100 s^{-1}. Dynamic tests results were compared with the results of static tensile tests carried out on specimens with identical geometry. The experimental results showed a significant increase of the tensile strength by increasing the strain rate. The tensile modulus and strain to failure were also observed to increase slightly by increasing the strain rate. It was also observed that the change from quasi-static to high dynamic loading condition caused an increase in energy absorption resulting in a larger damage region.

Compression test experiments were performed at strain rates of 10^{-3} and 450 s^{-1} by Ochola [4] to study the strain rate sensitivity of both carbon fiber reinforced polymer (CFRP) and glass fibre reinforced polymer (GFRP). The experimental dynamic test results were compared with static compression test data. The compressive stress–strain vs. strain rates data showed that the dynamic material strength for GFRP increases with increasing strain rates. The strain to failure for both CFRP and GFRP is seen to decrease with increasing strain rate. Depending on the loading rate, fiber kinking, which is prominent in GFRP coupled with the micro-buckling, and fibre fracture were observed at low strain rates while combination of global delamination, interfacial separation and spalling were observed at high strain rates, resulting in low strain to failure with high ultimate strength.

As noted by Tsai and Sun [5], the compressive strength of polymeric composites is rate-sensitive and that the presence of in-plane shear stress can appreciably lower the compressive longitudinal strength. Both low and high strain rate compression test was

performed and it is observed that failure was dominated by fiber micro-buckling at strain rates below $0.01s^{-1}$ and was dominated by matrix shear failure at higher strain rates for the 15° off axis specimen.

2. Experimental Test on Composites with a Circular Hole

Backlund and Aronsson [6] did static tension tests for the composite with holes and compared the results to the damaged zone model (DZM). A damage zone model (DZM), where the damage zone is modeled as a crack with loaded surfaces, has been evaluated with regard to its ability to predict tensile strength of carbon/epoxy laminates containing various types of holes.

The load-strain behaviour close to the hole edge becomes nonlinear at about half the fracture load, which suggests that damage initiates at this load level causing a more compliant material. It was also observed that close to the fracture load, damage occurred at the hole boundary in the 90^o and 45^o plies, while load carrying fibers were intact at the 0^o layer. However, at this load level, no damage in the form of delamination or matrix cracking was observed in the X-ray pictures. Post fracture inspection of the damage zones showed two interesting features. First of all, in the failure patterns of the 0° plies, it was observed that the damage initially grew along a curved path. Secondly, the damage zones at the hole boundary observed in the X-ray pictures were limited to a small volume and the shape was the same for both hole radii. The length of the damage zones, measured perpendicular to the load direction, was about 2–4 mm, which is almost the same as the predicted length at the maximum load. They concluded that based on the two fundamental parameters, unnotched tensile strength (σ_o) and apparent fracture energy G_c, the model excellently predicted the strength of notched laminates for a number of specimens tested.

Eriksson and Aronsson [7] further investigated the tensile strength of composites containing open holes by performing tension tests., They compared the experimental results with the point Stress Criterion (PSC), Damaged Zone Model (DZM) and Damaged Zone Criterion (DMC). They concluded that the DZC is simple to apply, makes

excellent predictions of the strength of specimens made from laminates of different configurations, and provides significantly improved accuracy compared with the PSC.

The effects of the hole size and the specimen width on the fracture behavior of different types of composites were experimentally investigated using tension testing by Jung-Kyu Kim, Do-Sik Kim and Nobuo Takeda [8]. The correlation drawn from the notched strength and the characteristic length was that the characteristic length decreased as the notched strength increased. The equivalent critical crack length corresponding to the damaged zone size was twice the characteristic length when the unstable fracture occurred. Thus, they modified the Point Stress Criterion (PSC) to predict the notch strength and it agreed with the experimental results.

Static compression testing with carbon fiber composites was conducted by Soutis and Fleck [9] with a single hole and un-notched coupon with a constant strain rate of 1mm/min. They investigated the effect of hole diameter on failure stress with a single hole of 6 – 15mm diameter. All the specimens failed through the hole at applied loads that decreased as the hole diameter was increased. Upon close examination of the damaged specimens, it showed that fiber micro-buckling occurred in the vicinity of the hole prior to catastrophic failure.

Guynn, Bradley and Elber [10] investigated the compressive failure in the damage zone of the composite under compressive loading. They noted that the experimental observations indicated that the Dugdale model did not accurately predict the load damage zone size relationship.

3. Analytical Strength Predication of Composite

It is desirable to be able to predict the performance of a particular lay-up of a given material based on some set of material properties. Failure theories are used to calculate the un-notched characteristics of multi-directional composite laminates which can be extremely in depth as some were considering the micro-mechanical interactions of fiber, matrix, and interface [11].

As highlighted in the recent World-Wide Failure Exercise [12], substantial effort has gone into generating these theories. The study compared 18 current theories of predicting failure in un-notched composite laminates, and evaluated each based on 14 test cases. While no single theory worked best for all conditions, several performed relatively well for laminates consisting of 0°, ±45°, and 90° plies, which is typical of laminates used in aerospace applications. The Maximum Stress Criteria, Tsai-Wu Criteria and Hashin Criteria are considered in the study based on their simplicity and performance in the exercise. Failure criteria can be thought of as the combination of stresses necessary to cause loss of structural integrity of the laminate. Therefore, for every composite system, there is a safe operating region or envelope, inside which failure does not occur. Failure theories seek to generate these envelopes using strength of the composite, typically longitudinal tensile strength, longitudinal compressive strength, transverse tensile strength, transverse compressive strength, and in-plane shear strength.

None of these failure criteria considered the rate effect of the material which is very important for the polymer matrix composites. The properties of the polymer matrix composites vary with strain rate. In order to better represent the failure behavior of polymer matrix composites, the rate effect of the material properties has to be considered in the failure criteria.

a. Maximum Stress Criteria

This is one of the earliest and easiest to implement failure criteria for multi-directional laminates. For the Maximum Stress Criterion [13], each and every one of the principle stresses must be less than the respective strengths. Failure envelopes are generated by the equations for tensile stresses

$$\sigma_1 < X_t, \ \sigma_2 < Y_t \tag{1}$$

for compressive stresses,

$$\sigma_1 > X_c, \ \sigma_2 > Y_c \tag{2}$$

and also,

$$|\tau_{12}| < S \tag{3}$$

These conditions are applied for each lamina, and as long as the applied stress in any lamina remains inside the three-dimensional space defined by the failure envelope, the theory does not predict failure. A severe limitation of this approach is that there is no interaction between the modes of failure. A laminate under combined loading is assumed to perform exactly the same as a laminate under uniaxial loading. This is referred to as a non-interactive failure theory. A similar approach, called the Maximum Strain Criteria, is identical in implementation except that it is based on strains, not stresses. The failure envelopes are generated by the equations

$$\varepsilon_1 < X_{\varepsilon_t},\ \varepsilon_2 < Y_{\varepsilon_t},\ |\gamma_{12}| < S_{\varepsilon} \tag{4}$$

$$\varepsilon_1 > X_{\varepsilon_c},\ \varepsilon_2 > Y_{\varepsilon_c} \tag{5}$$

b. Tsai-Wu Criterion

The Tsai-Wu criterion [14] predicts that failure will occur when the following equation is satisfied for the case of an orthotropic lamina under the plane stress condition:

$$F_1\sigma_1 + F_2\sigma_2 + F_6\sigma_6 + F_{11}\sigma_1^2 + F_{22}\sigma_2^2 + F_{66}\sigma_6^2 + 2F_{12}\sigma_1\sigma_2 = 1 \tag{6}$$

F_{ij} are the strength tensors of the second and fourth rank, respectively, and when under tensile and compressive load, they can be expressed as the following equations

$$F_1 = \frac{1}{X_t} + \frac{1}{X_c},\quad F_{11} = -\frac{1}{X_t X_c} \tag{7}$$

$$F_2 = \frac{1}{Y_t} + \frac{1}{Y_c},\quad F_{22} = -\frac{1}{Y_t Y_c} \tag{8}$$

Upon simplification, the failure criterion becomes

$$\frac{\sigma_1^2}{X^2} + 2F_{12}\sigma_1\sigma_2 + \frac{\sigma_2^2}{Y^2} + \frac{\tau_{12}^2}{S^2} = 1 \tag{9}$$

F_{12} can be solved after substituting Equation (7) and (8)

$$F_{12} = \frac{1}{2\sigma^2}\left[1 - \left[\frac{1}{X_t} + \frac{1}{X_c} + \frac{1}{Y_t} + \frac{1}{Y_c}\right]\sigma + \left[\frac{1}{X_t X_c} + \frac{1}{Y_t Y_c}\right]\sigma^2\right] \tag{10}$$

The value of F_{12} depends on the various engineering strengths plus the biaxial tensile failure stress, σ.

The Tsai-Wu criterion has been widely used because of its user-friendliness and accuracy. It also has graphical interpretations of the results facilitated by the formulation of the tensors and an improved curve-fitting capability due to the additional term, F_{12}. However, one of the disadvantages of this method is the absence of failure mode indicators. For example, implementation of the Maximum Stress Criteria can indicate whether failure is due to longitudinal compression or transverse tension. The Tsai-Wu criterion has no such feature. Nevertheless, the Tsai-Wu criterion remains a popular tool that is generally accepted as providing decent results.

c. Hashin Failure Criteria

Hashin [15] proposed failure criteria that consider the effects of stress interaction and include the failure mode and load direction in determining strength. It is defined by the following four distinct failure mode equations.

Tensile Fiber Mode: $$\left(\frac{\sigma_{11}}{X_t}\right)^2 + \frac{1}{S_c^2}\left(\sigma_{12}{}^2 + \sigma_{13}{}^2\right) = 1 \tag{11}$$

Fiber Compressive Mode: $$\left|\sigma_{11}\right| = X_c \tag{12}$$

Tensile Matrix Mode: If $(\sigma_{22} + \sigma_{33}) > 0$, then

$$\frac{1}{Y_t^2}(\sigma_{22} + \sigma_{33})^2 + \frac{1}{S_t^2}(\sigma_{23}{}^2 - \sigma_{22}\sigma_{33}) + \frac{1}{S_c^2}(\sigma_{12}{}^2 - \sigma_{13}{}^2) = 1 \tag{13}$$

Compressive Matrix Mode: If $(\sigma_{22} + \sigma_{33}) < 0$, then

$$\frac{1}{Y_c}\left[\left(\frac{Y_c}{2S_c}\right)^2 - 1\right](\sigma_{22}+\sigma_{33}) + \frac{1}{4S_t^2}(\sigma_{22}+\sigma_{33})^2 + \frac{1}{S_t^2}(\sigma_{23}{}^2 - \sigma_{22}\sigma_{33}) + \frac{1}{S_c^2}(\sigma_{13}{}^2 + \sigma_{13}{}^2) = 1 \quad (14)$$

where σ_{13} and σ_{23} are the out-of-plane shear stresses of the laminate, σ_{33} is the stress of the laminate in the thickness direction, and S_t is the transverse shear strength.

The Hashin criteria are semi-interactive, in which the normal and shear stress factors are considered in the determination of each failure mode, but not all stress components are considered for each mode. The interaction of stresses can be a significant factor in composite strength. Thus, these criteria are an improvement over the maximum stress criterion. The indication of the failure mode may also make it more desirable than the Tsai-Wu Criterion for some applications.

4. Analytical Strength Prediction of Composite with a Circular Hole

The introduction of notches or stress concentrations into a composite laminate can greatly reduce the strength of a structure. As such, notched strength prediction is an active area of research within the composites community. Given the anisotropy, diversity of damage modes, and complex failure progressions found in composites; strength prediction can be very difficult, and no clear agreement exists as to the best way to perform analysis. There are several methods, which include the extension of linear elastic fracture mechanics, typically used in metallic materials, to mechanics of materials analysis, to detailed finite element techniques that attempt to include micromechanical details and simulate individual damage modes. Each technique has its own pros and cons and is also comprised of differing assumptions, effort, and knowledge of material properties.

a. Waddoups, Eisenmann, and Kaminski Failure Theory

One of the earliest attempts at notched strength prediction of composite laminates was the Waddoups, Eisenmann, and Kaminski (WEK) failure theory [16]. The WEK method is an application of Linear Elastic Fracture Mechanics (LEFM) to

composite materials. It is logical that early attempts at failure prediction in composites would be an extension of the methods used in metallic materials. Wu [17] found this application was suitable when three conditions were met.

- The orientation of the flaw with respect to the principal axis of symmetry must be fixed.
- The stress intensity factors defined for anisotropic cases must be consistent with the isotropic case in stress distribution and in crack displacement modes
- The critical orientation coincides with one of the principal directions of elastic symmetry

The basis for the WEK model is the replacement of damage at the notch with an intense energy region, shown in Figure 1. As mentioned earlier, the progression of damage in composite laminates is complex and can comprise of multiple damage types. The WEK method evades the need to predict each damage type in the laminate by using this intense energy region.

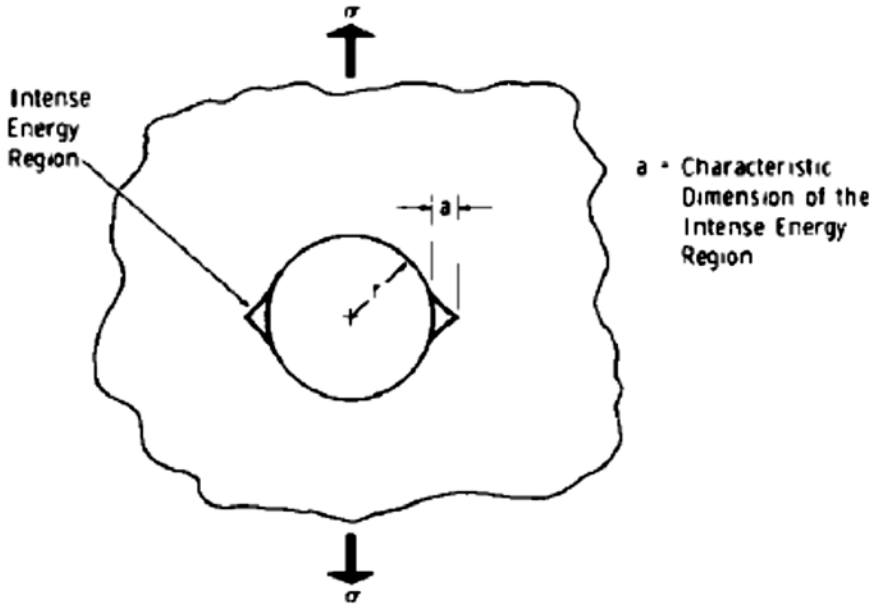

Figure 1. WEK fracture model, from [16]

Waddoups, Eisenmann, and Kaminski applied the work of Irwin [18] by relating the energy release rate G_I to the stress intensity factor K_I using the equation

$$G_I = \frac{(1-\upsilon)\pi}{2G} K_I^{\,2} = \frac{(1-\upsilon^2)\pi}{E} K_I^{\,2} \tag{15}$$

where G is the Modulus of Rigidity, E is the Modulus of Elasticity and υ is the Poisson's ratio.

For a characteristic length "a" that is small and finite, the effect of damage zone size can be analyzed by the stress intensity factor solution developed by Bowie [18] for the problem of cracks growing from a circular hole in an isotropic plate. Paris and Sih [19] found the solution to this geometry to be

$$K_I = \sigma_N^{\infty} \sqrt{\pi a}\, f\left(\frac{a}{R}\right) \tag{16}$$

Combining Equation (15) and (16) yields:

$$\sqrt{G}_I = \left[\pi \sqrt{\frac{a\left(1-\upsilon^2\right)}{E}}\right] \sigma\, f\left(\frac{a}{r}\right) \tag{17}$$

The authors then assume that the material is ideally brittle with constant G_I. Additionally, it is assumed that the change in the characteristic length "a" is small compared to the hole radius. Thus the equation can be rearranged to show

$$\frac{\sqrt{G_I}}{\left[\pi \sqrt{\frac{a\left(1-\upsilon^2\right)}{E}}\right]} = \sigma\, f\left(\frac{a}{r}\right) \simeq Const \tag{18}$$

This allows the ratio of un-notched and notched strengths to be written as

$$\frac{\sigma_0}{\sigma_N^{\infty}} = f\left(\frac{a}{R}\right) \tag{19}$$

Values of f(a/R) have been found by Paris and Sih [20]. Thus, for any value of "a," the ratio of notched to un-notched strengths can be calculated for differing hole radii. The assumptions used in applying LEFM to composites deserve attention. The assumption that flaw orientation remains fixed seems unlikely given the variety of

damage mechanisms that occur. Additionally, it is not likely that the stress distribution in an anisotropic composite would be consistent with the isotropic case.

b. Whitney-Nuismer Failure Theory

The Whitney-Nuismer method [21] postulates that failure of a notched laminate occurs when the stress at some characteristic distance away from the notch reaches the un-notched strength of the laminate. The Whitney-Nuismer method can be implemented via either the "Point Stress" Criterion or the "Average Stress" Criterion, shown schematically in Figure 2 and Figure 3, respectively [22].

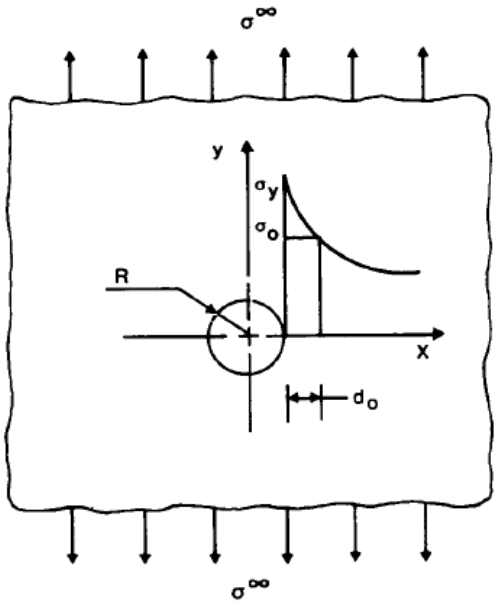

Figure 2. Schematic representation of the "Point-Stress" criterion for a laminate containing a circular hole, From [22].

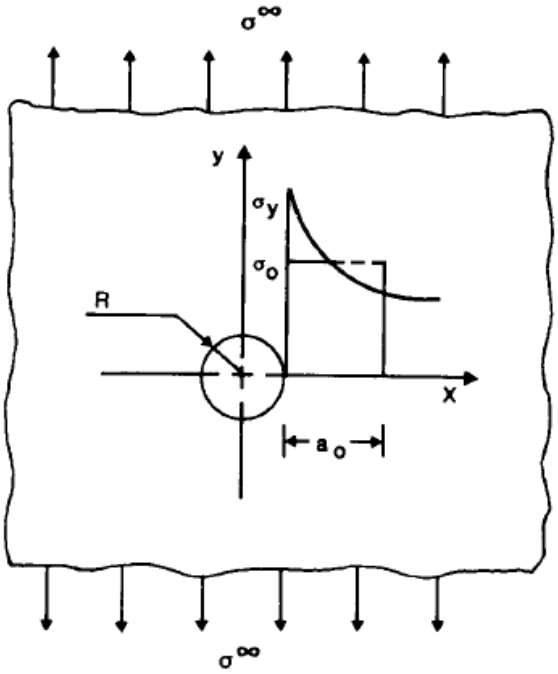

Figure 3. Schematic representation of the "Average-Stress" criterion for a laminate containing a circular hole, From [22].

The Point Stress Criterion assumes that failure fracture occurs when the stress at the characteristic distance d_o is equal to or greater than the un-notched strength of the laminate, given by the equation

$$\sigma_y(x,o)\Big|_{x=R+d_o} = \sigma_o \tag{20}$$

The Average Stress Criterion assumes that fractures occur when the average stress over some characteristic distance a_o is equal to or greater than the un-notched strength of the composite, and is given by the equation

$$\sigma_o = \frac{1}{a_o}\int_R^{R+a_o} \sigma_y(x,o)\,dx \tag{21}$$

Whitney and Nuismer sought to address the effect of notch size in laminated composites. Timoshenko [23] originally showed the dependence of the normal stress σ_y on hole size in an infinite, isotropic material to be

$$\frac{\sigma_y}{\sigma^\infty} = 1 + \frac{1}{2}\left(\frac{R}{x}\right)^2 + \frac{3}{2}\left(\frac{R}{x}\right)^4 \tag{22}$$

This results in the stress distribution shown in Figure 4.

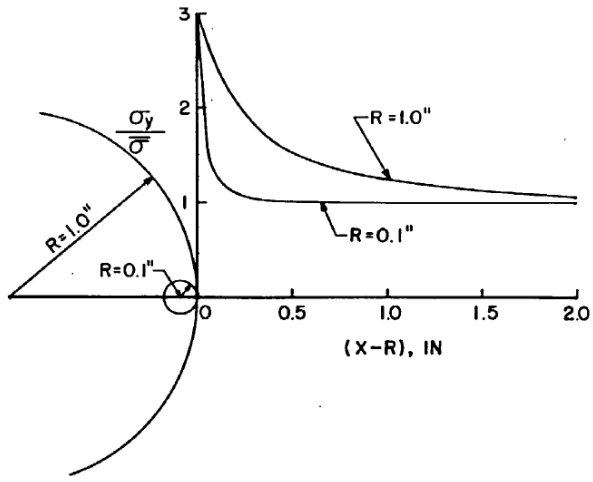

Figure 4. Stress distribution for a hole in an infinite isotropic plate, From [21]

This approximation is valid for quasi-isotropic laminates with a stress concentration factor $K_T^\infty = 3$, but is inaccurate for orthotropic laminates, where $K_T^\infty \neq 3$. Konish and Whitney [24] extended Timoshenko's work to an orthotropic plate under a uniform uniaxial stress, showing the normal stress σ_y to be

$$\sigma_y(x,0) = \frac{\sigma^\infty}{2}\left\{2 + \left(\frac{R}{x}\right)^2 + 3\left(\frac{R}{x}\right)^4 - \left(K_T^\infty - 3\right)\left[5\left(\frac{R}{x}\right)^6 - 7\left(\frac{R}{x}\right)^n\right]\right\}, x > R \tag{23}$$

Lekhnitskii's solution for the stress concentration factor for an open hole in an anisotropic plate [25] can be used with the equation

$$K_T^\infty = 1 + \left\{2\left[\left(\frac{E_y}{E_x}\right)^{1/2} - \upsilon_{yx}\right] + \frac{E_y}{G_{yx}}\right\}^{1/2} \tag{24}$$

When this stress distribution is applied to the Point Stress Criterion, the ratio of the notched to un-notched strength is given by

$$\frac{\sigma_N^{\infty}}{\sigma_o} = \frac{2}{\left\{2+\xi_1^2+3\xi_1^4-\left(K_T^{\infty}-3\right)\left(5\xi_1^6-7\xi_1^8\right)\right\}} \tag{25}$$

where

$$\xi_1 = \frac{R}{R+d_o} \tag{26}$$

Similarly, applying the stress distribution to the Average Stress Criterion yields

$$\frac{\sigma_N^{\infty}}{\sigma_o} = \frac{2\left(1-\xi_2\right)}{\left\{2-\xi_2^2-\xi_2^4+\left(K_T^{\infty}-3\right)\left(\xi_2^6-\xi_2^8\right)\right\}} \tag{27}$$

where

$$\xi_2 = \frac{R}{R+a_o} \tag{28}$$

Similar to the WEK model, the Whitney-Nuismer model uses two considerations, the un-notched strength of the laminate and the characteristic distance, to predict the strength of the notched laminate. The characteristic distance is determined experimentally and was used together with the data for curve fitting. One advantage of the Whitney-Nuismer model over the WEK method is the prediction of notched strength without the application of linear elastic fracture mechanics. As discussed earlier, LEFM is questionable in its applicability, and the Whitney-Nuismer Point Stress and Average Stress Criteria offer a significant improvement in the study of fracture in composites.

c. Damage Zone Model or Cohesive Zone Model

Early notch strength prediction techniques were mainly based on the calculation of a stress field based on the material properties of the undamaged composite laminate, and failure was determined based on some experimentally method. They provide little understanding in composite damage growth.

Meticulous modeling is difficult and expensive because damage progression is complex and the variety of damage modes exist in composite materials. Therefore, Damage Zone Model [26] uses the fracture energy G_C* to account for all energy dissipated by the various damage mechanisms. This model was originally used by Hillerborg et al [27] for analysis of concrete. For a notched composite subjected to an external load, damage can occur in the region adjacent to the notch, as shown in Figure 5.

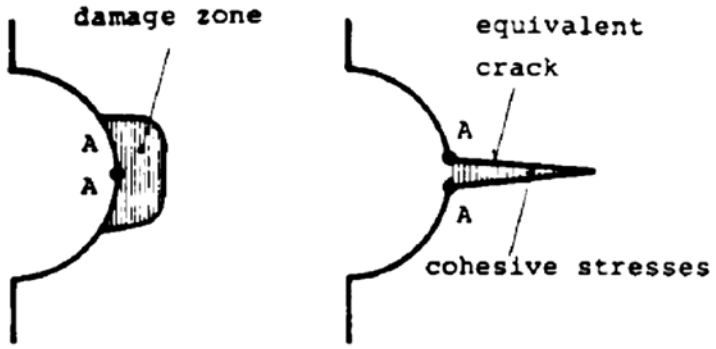

Figure 5. Damage zone at notch and Equivalent crack, From [6]

This damage zone is replaced by a fictitious or equivalent crack, and analyzed via a Dugdale - Barenblatt method, with cohesive stresses acting on the crack face as shown in Figure 6. The damage increases in the material as the load increases, which are modeled as the increased crack opening and longer crack length. In general, the relationship between stress and displacement is assumed linear, as shown in Figure 6. Other relationships can be selected based on the material. The unloaded material has no equivalent crack if there is no damage. As damage increases, the cohesive stresses decrease, with material softening occurring due to damage. With this approach, stress redistribution and stiffness degradation can be calculated with classical or finite element methods.

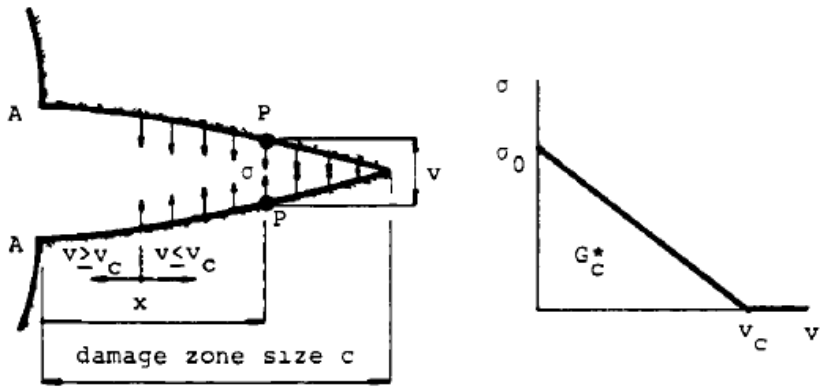

Figure 6. Dugdalel/Barenblatt cohesive zone: (a) crack with opening v(x), cohesive stress a(x), and length c; (b) assumed linear relation between a and v, From [6]

It should be noted that Soutis et al. [9, 28] have successfully applied the cohesive zone model to the open hole compression, substituting the kink band region and delaminated area with the equivalent crack.

For a variety of geometries, lay-ups, thickness, and notch sizes, there seems to have excellent agreement between experimental and analytical predictions for both strength and damage progression using the above technique. However, complex finite element analysis is required, and substantial computational effort will be required to obtain convergence.

C. OBJECTIVES OF RESEARCH

The objective of the thesis is to examine the progressive damage/failure of composite panels with holes under progressive axial loading. In other words, a series of experiments are conducted to examine the progressive damage/failure initiating from the notch tip to complete fracture under tensile and compressive loading, respectively. Additionally, the study is to investigate the strain rate effect on the strength and stiffness of perforated specimens. Especially, to the author's best knowledge, there is no study for un-notched and perforated composite strength under non-uniform varying strain rate loading. As a result, this research studies the effect of non-uniform varying strain rates on the un-notched and perforated composite specimens.

II. EXPERIMENTAL SETUP AND PROCEDURES

Following is a description of the experimental equipment, techniques and procedures used over the course of this research. The material, lay-ups, and specimen configurations are described. This is followed by a brief description of the Vacuum-Assisted Resin Transfer Molding procedures for fabricating of composite coupons. Finally, description of the equipment used for the un-notched tension and compression tests, perforated tension, and perforated compression is detailed. Video recording was done for all the experiments performed to validate the failure modes.

A. COMPOSITE SAMPLE CONSTRUCTION

1. Materials

The composite samples were fabricated from E-glass and Derakane 510A vinyl ester resin. The E-glass used for this study is an 8.9oz per square yard, bi-directional fiberglass E cloth. It is chosen as it is tightly woven, high performance and has a high strength to weight ratio. This material was also used mainly in advanced composite laminates.

The Derakane resin was mixed with Methyl Ethyl Ketone Peroxide (MEKP) 1.25 percent, Cobalt Napthenate (CoNAP) 0.2 percent solution, and N, N- Dimethylaniline (DMA) 99.5 percent to achieve an approximately one-hour cure time. The cure time must be kept to one hour or less to avoid air bubble formation in the sample. All components are mixed based on a percent weight for a nominal one-hour cure time per manufacturer's directions. MEKP was used as the initiator for the curing reaction. If the sample is prepared at a temperature of 70ºF or greater, the CoNAP alone acts as the reaction catalyst and is therefore responsible for determining cure time. If the sample must be prepared at a temperature less than 70ºF, DMA must be added in addition to CoNAP to achieve a one-hour cure time. The amounts of MEKP, CoNAP, and DMA are used only to change the gel time, and have no effect on the composite strength.

Figure 7. E-glass

(a) (b)

Figure 8. (a) Methyl Ethyl ketone peroxide (MEKP) (b) cobalt napthenate (CoNAP)

Figure 9. Derakane resin

2. Test Specimen Geometries

There were two different sets of coupons constructed during this research. The construction process is the same for both, but the number of ply of the E-glass fiber is different to achieve different thickness. For tension test, the 2mm thick coupon will be cut into smaller specimens. The dimensions of the specimens are given in Figure 10 and Figure 11.

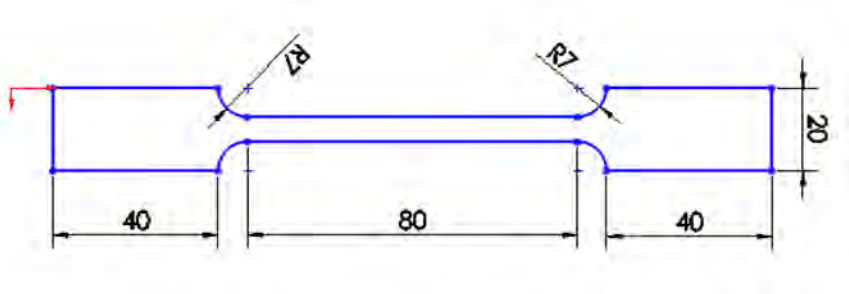

Figure 10. Dimension of tension test un-notched specimens. All dimensions in millimeters.

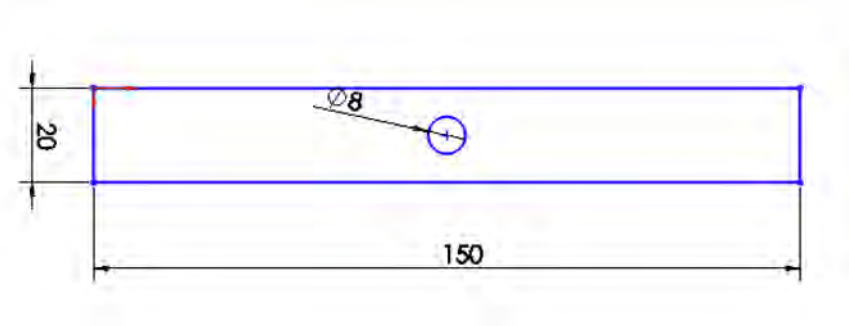

Figure 11. Dimension of tension test perforated specimens. All dimensions in millimeters.

For the compression tests the 4mm thick coupon is cut into smaller specimens. The dimension of the specimens is given in Figure 12 and Figure 13.

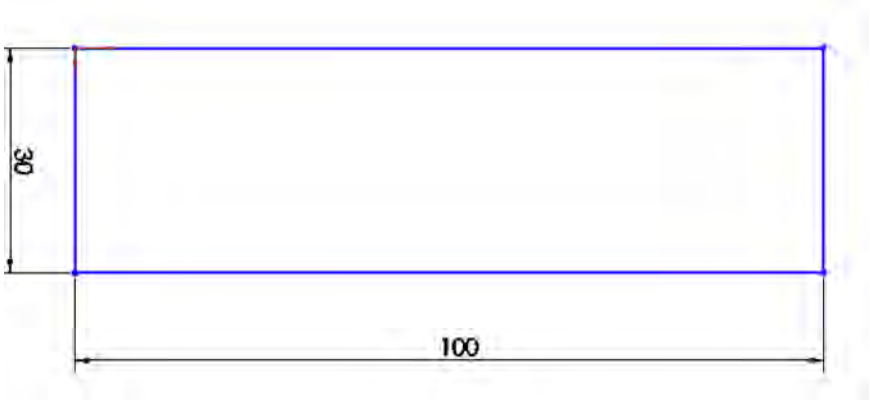

Figure 12. Dimension compression test un-notched specimens. All dimensions in millimeters.

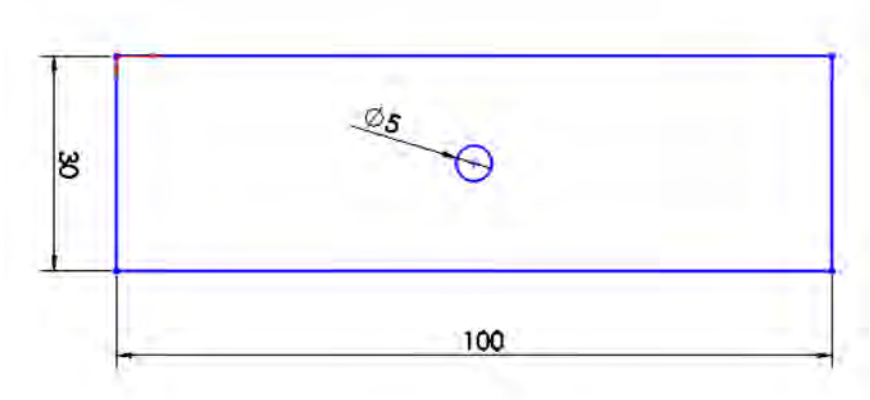

Figure 13. Dimension compression test perforated specimens. All dimensions in millimeters.

3. Vacuum-Assisted Resin Transfer Molding (VARTM)

Vacuum-Assisted Resin Transfer Molding is a process which involves placing dry fibers in a mold and adding the resin separately. The resin is injected in the mold at the inlet port until it flows out the outlets and the fibers become completely wetted out. The mold is composed of a single flow surface and a vacuum bag. A vacuum bag is just a thin film that covers the fiber preform and is connected to the base of the mold, or it may encompass the entire mold. A vacuum is then pulled on the part in order to impart a one atmosphere pressure over the part surface. This process provides for a large reduction in cost because purchasing the fibers and resin separately is cheaper than prepreg materials,

and vacuum bags are much cheaper than an autoclave, if using the autoclave production method. Additionally, cure times are faster because a catalyst is used in VARTM as an alternative to waiting for the system to get to really high temperatures.

This technique was used to fabricate the composite coupons for this study and is the same as Klopfer [29] when he was doing his thesis study in Naval Postgraduate School. The VARTM which was used in this study consist of five main components, namely the vacuum pump, gauge board, resin trap, glass surface and the resin reservoir as shown in Figure 14.

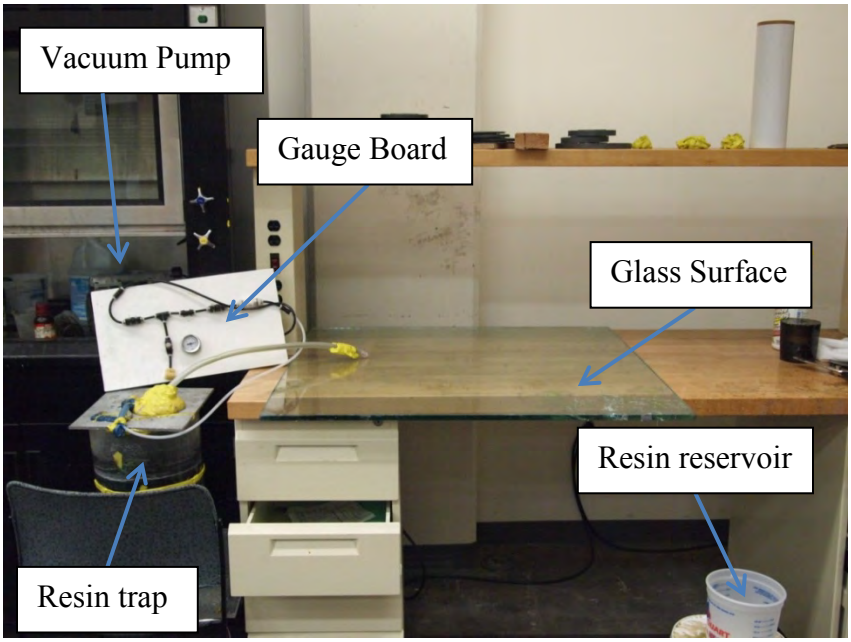

Figure 14. Main components of the VARTM.

The vacuum pump draws the resin from the resin reservoir through the coupon and into the resin trap. It is very important to ensure that there is no air within the composite coupon and there is no air leakage. This is ensured by having the gauge board which was used to measure the vacuum pressure in the system. If there is any air leakage within the system, pressure will drop and will be reflected by the vacuum pressure gauge.

During the process, the vacuum pump will draw the residual resin through the coupon and into the resin trap. The resin trap collects the residual resin that was drawn through to prevent the contamination of the vacuum pump and gauge board.

A 0.5 inch thick glass surface was used to provide as a molding surface for the composite coupon. It gives a good sealing effect and has an ease of cleaning as well. The resin reservoir was a plastic bucket that was used to mix the resin and allow the polyethylene tubing to be inserted once the suction pressure is achieved.

4. Composite Fabrication Procedure

The procedure is similar to Klopfer [29] but simpler, as there are not any metal wire sheets to be placed in between the E-glass ply. In this section, a brief description of the procedure will be given. The number of layers of the E-glass is the only difference for each composite coupon formed. The fabricate procedure can be break down into five steps:

i) Coupon preparation

ii) Setup of the vacuum bag

iii) Resin preparation

iv) Resin transfer

v) Cleaning up

a. Coupon Preparation

The numbers of E-glass layers required is cut into 30mm long by 30mm wide. The coupon for tension test will require 10 plies, while the coupon for compression test will require 20 plies. Two pieces of the Resin Infusion Flow Netting is cut to 40mm long and 35mm wide and another two pieces of the Econolease peel ply is cut to 50mm long by 40mm wide. One important point is that there must be sufficient space for the 0.5 inch helical polyethylene tubing to be placed on the top and bottom of the Resin Infusion Flow Netting.

The first layer will be a Resin Infusion Flow Netting, follow by the Econolease peel ply and then the E-glass layers. Subsequently, the Econolease peel ply will be placed on top of the E-glass layers follow by the Resin Infusion Flow Netting.

Figure 15. Cutting of the e-glass layers.

b. Setup of the Vacuum Bag

The glass surface has to be inspected to ensure that it is clean. Two pieces of the Teflon film of 50mm long and 30mm wide is cut and placed on the glass surface for easy removal and act as a protective layer. The layers of coupon are placed on top of the Teflon film and a rectangular shape is created around the Teflon film using the AT-200Y sealant tape as shown in Figure 16.

Figure 16. Setting up of the vacuum bag.

Two pieces of the 0.5 inch polyethylene tubing is cut. One will be used to transfer the resin from the resin reservoir to the vacuum bag and composite coupons, so the length has to be determined appropriately. The other piece of the tubing is used to draw the resin from the vacuum bag and composite coupon so appropriate length has to be determined from the resin trap to the coupon. Two pieces of the helical tubing is cut and one is placed and secured with duct tape at one end of the top polyethylene tubing. The other end of the helical tube is duct taped to prevent the sharp edges from puncturing a hole in the vacuum bag. As for the bottom edge of the coupon, similar steps are followed.

The helical tube at the bottom edge is placed in between the bottom Resin Infusion Flow Netting and the Econolease peel ply. This is to ensure complete resin saturation as the resin was drawn from the bottom edge and surface, to the top edge and surface through the pressure difference.

A piece of the Dahlar® Vacuum Bag of 100mm long and 80mm wide is cut and placed on top of the sealant tape as shown in Figure 17. Special care has to be taken to ensure minimum air leakage at the corners and the joint area as shown in Figure 18.

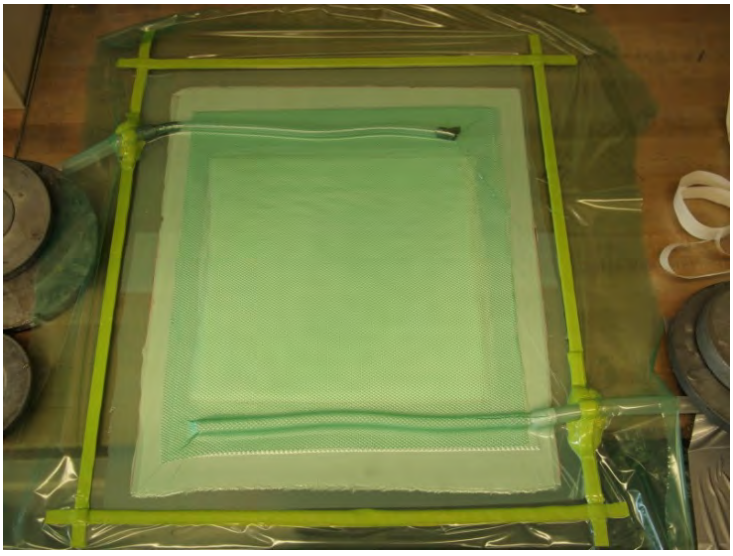

Figure 17. Vacuum bag assembly.

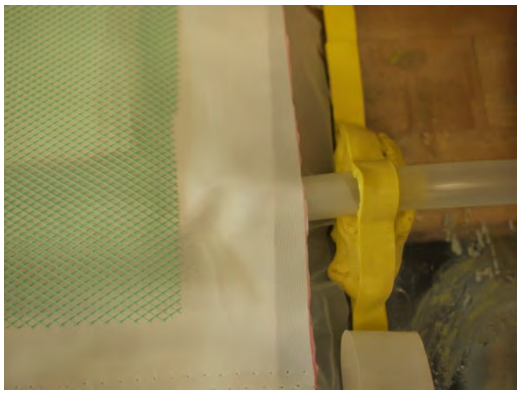

Figure 18. Proper sealing of the joint area at bottom edge.

The end of the tubing leading to the resin reservoir is plugged with the vacuum sealant tape as shown in Figure 19. The vacuum pump is switched on subsequently and a pressure of 30psi has to be maintained. The pressure can be read from the pressure gauge at the gauge board.

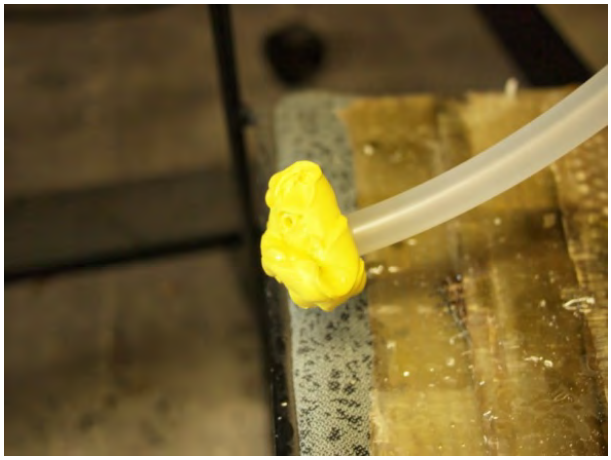

Figure 19. Sealant tube plugged onto the tubing leading to the resin reservoir.

c. Resin Preparation

1.25 liters of Derakane 510A resin was poured into the resin reservoir. 15.6ml of MEKP is added into the resin and stirred with a paint stirrer to ensure that the mixture is well mixed before the 3.125ml of CoNAP is added to the resin mixture. The mixture is then stirred again and remains to rest for 10 minutes as shown in Figure 20.

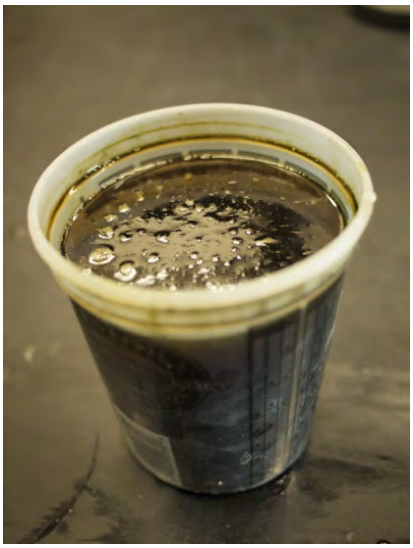

Figure 20. Resin Mixture.

d. Resin Transfer

After 10 minutes, the resin reservoir is placed in position 5, as shown in Figure 14. The polyethylene tube is submerged into the resin and the sealant tape used to plug the vacuum tubing is removed. This step is important and have to be done with the tube submerged is to ensure no air leakage into the vacuum bag as shown in Figure 21.

Figure 21. Polyethylene tube submerged in the resin reservoir with sealant tape removed.

The resin will flows through the coupon as shown in Figure 22. Once the coupon is fully saturated with resin and the resin in the resin reservoir starts to harden as shown in Figure 23, the plastic tube submerge inside the resin can be plugged with the sealant tube again. This is to break the transfer process and the setup is left to cure for 24 hours.

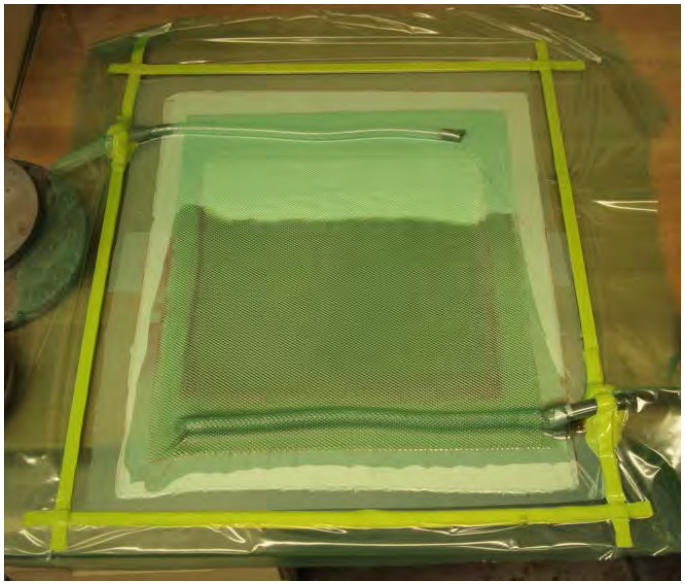

Figure 22. Resin flowing through the coupon.

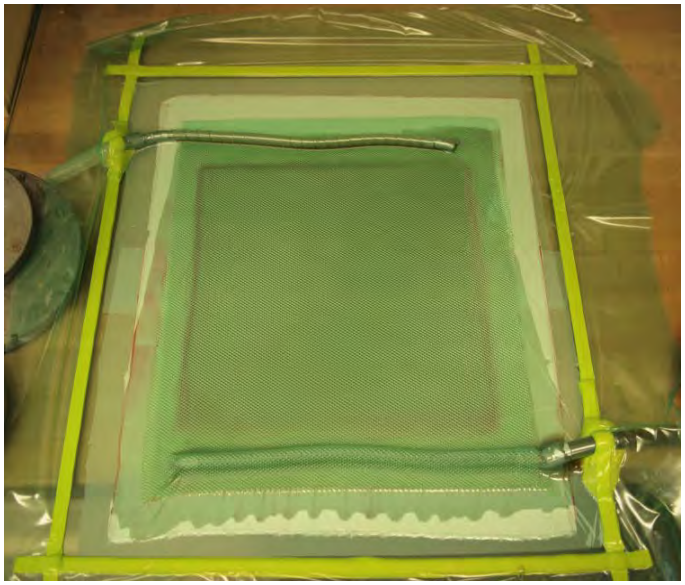

Figure 23. Coupon fully saturated with resin.

e. Cleaning Up

After 24 hours of curing, the vacuum bag is removed from the glass surface and all the tubing can be detached. The glass surface has to be cleaned thoroughly. By peeling off the Econolease peel ply, the condition of coupon can be inspected.

B. TESTING EQUIPMENT AND PROCEDURES

1. Compression Test

The compression test is performed using the Instron® 4507 Universal Material Testing machine which has a 20kN load cell as shown in Figure 24. The Series IX Instron software is used to control the load frame and provides data generated from the tests. The limitation of the experiments is the maximum crosshead speed of 500mm/min which greatly restrict the maximum strain rate that can be tested. Emery cloth of 150grit was placed in the grip to give the gripped surface a uniform pressure distribution and also to provide enough friction to stop slipping. Two aluminum alignment plates as shown in Figure 25 were also machined and place in the grip to ensure that the gauge length is constant.

Figure 24. Instron® 4507 universal material test machine.

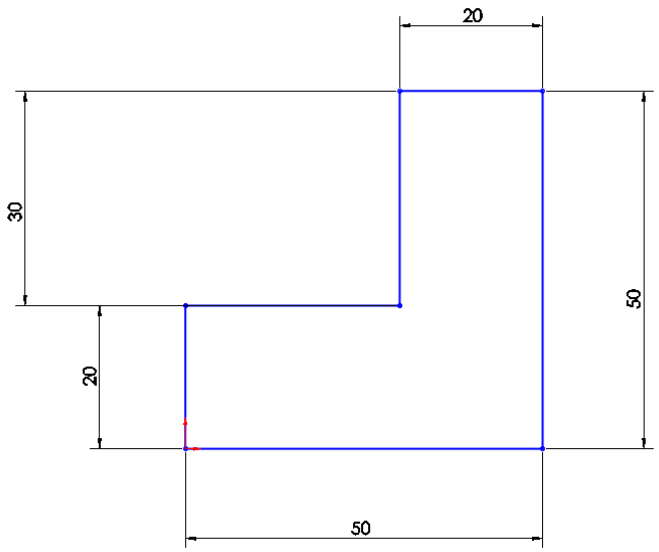

Figure 25. Dimension of alignment plate for compression test. Thickness of 3.95mm. All dimensions in millimeters.

The applied strain rate for the compression test is varied from $0.001s^{-1}$ to $0.2s^{-1}$. Table 1 shows the crosshead speeds used during the test which was derived from the following equation

$$\dot{\varepsilon} = \frac{V}{l_o} \tag{29}$$

Table 1. The applied strain rate and crosshead speed for compression test

	Strain rate (per sec)	Gauge Length (mm)	Crosshead Speed(mm/sec)
1	0.001	40	0.04
2	0.01	40	0.4
3	0.1	40	4
4	0.2	40	8

All the experiments are repeated and consistency is verified between two to three sets of data. The parameters are thereafter computed as the average. The specimens are loaded in compression to failure at each crosshead speed.

2. Tension Test

The tension test is performed using the Instron® 4507 Universal Material Testing machine which has a 20kN load cell as shown in Figure 24. This is the same machine that was utilized for the compression test. The same software used to control the load frame to perform various types of loading test.

For the start of each experiment, measurement of the gauge length is performed to ensure a constant 80mm. In order to make sure that there is no slippage of the specimen since it often occurs during tension test, emery cloth of 150 grits is placed in the grips to provide enough friction to stop slippage. The applied strain rate for the tension test is varied from $0.0005s^{-1}$ to $0.05s^{-1}$. Table 2 and Table 3 show the crosshead speeds used during the test. The specimens are loaded in tension to failure at each crosshead speed.

Table 2. The applied strain rate and crosshead speed for perforated tension specimen.

	Strain rate (per sec)	Gauge Length (mm)	Crosshead Speed(mm/sec)
1	0.0005	90	0.045
2	0.005	90	0.45
3	0.05	90	4.5

Table 3. The applied strain rate and crosshead speed for un-notched tension specimen.

	Strain rate (per sec)	Gauge Length (mm)	Crosshead Speed(mm/sec)
1	0.0005	80	0.04
2	0.005	80	0.4
3	0.05	80	4

3. Varying Strain Rate Test

In addition to the static tension and compression tests performed with constant strain, another set of tests were carried out where the strain rate was changed during each test. The tests were performed using the Instron® 4507 Universal Material Testing machine. The test started out with an initial crosshead speed and it was kept constant before it went through a step change in the crosshead speed to the second speed where it was kept constant until the specimen failed. The transition strain is a half of the specimen failure strain which were acquired from the first set of tension and compression test. This test was performed for both tension and compression, and also for un-notched and perforated specimens. Table 4 and Table 5 tabulate the corresponding strains and the transition strain for the tests.

Table 4. Varying strain rate parameters for compression tests.

		First Strain rate (per sec)	Second Strain rate (mm)	Transition Strain
Un-notched	1	0.001	0.2	0.0275
	2	0.2	0.001	0.0297
Perforated	1	0.001	0.2	0.0289
	2	0.2	0.001	0.0356

Table 5. Varying strain rate parameters for tension tests.

		First Strain rate (per sec)	Second Strain rate (mm)	Transition Strain
Un-notched	1	0.0005	0.05	0.0138
	2	0.05	0.0005	0.0223
Perforated	1	0.0005	0.05	0.009801
	2	0.05	0.0005	0.01196

THIS PAGE INTENTIONALLY LEFT BLANK

III. RESULTS AND DISCUSSION

This chapter presents the results of the various tests performed on the composite laminates. The un-notched test performed is to enhance the understanding of the composite under various strain rates, and to gather baseline data to assist in the validation of the predication of perforated specimens.

The test results are grouped first according loading type, the varying strain rate loading and its effect, and then comparison of experimental results with Whitney-Nuiser Failure Prediction Theory, namely the Point Stress Criterion and Average Stress Criterion, which was mentioned in Chapter I. The findings from the un-notched compression data will be presented first, followed by perforated compression, un-notched tension, and perforated tension tests. For each test type, data will be presented first in graphical form, which shows the comparisons of the strengths of the composite laminates at different strain rates. This will be followed by a detailed description of the composite progressive failure behavior, and the results of the visual inspection and optical microscope.

A. UN-NOTCHED COMPRESSION

The ultimate compressive stresses and compressive strain of the un-notched specimens with different strain rate for compression test are shown in Figure 26.

The compressive stress and strain increase as the strain rate increases. It is also noted that there is a nonlinear curve for some strain rate at early stage of loading. This is more evident when the specimen is subjected to a lower strain rate, and as the strain rate increases, the slope is generally more linear. This could be due to the laminate matrix cracking for the initial phase and subsequently the fiber is subject to loading during which the trend increases linearly. A further investigation will be conducted later to better understand such a nonlinear curve in the beginning.

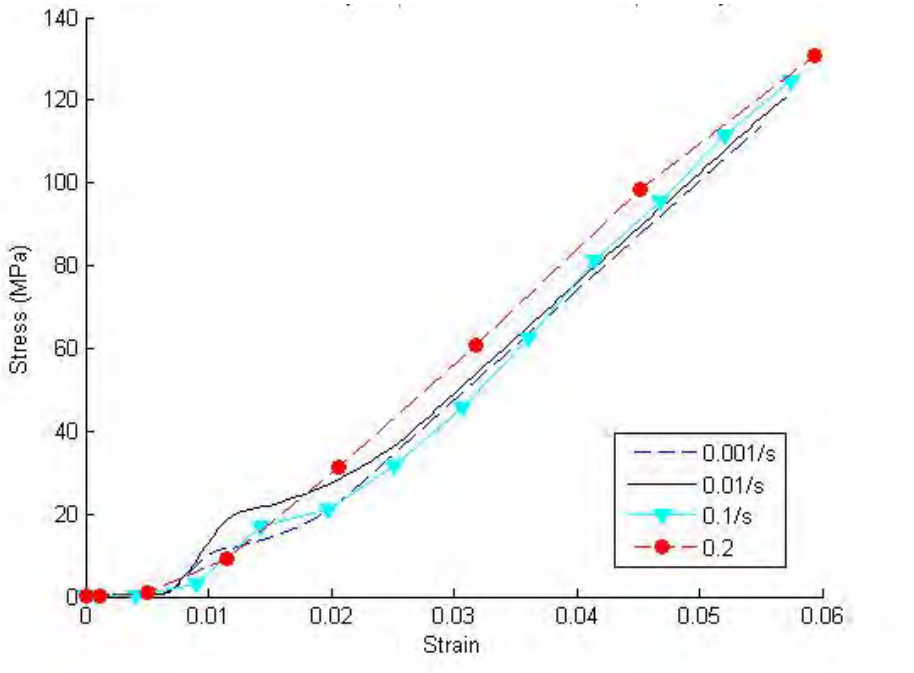

Figure 26. Compressive stress and strain relationship for un-notched specimens.

The following is a discussion of the visual observation during the tests and the inspection of the specimens after the experiment visually using an optical microscope.

The failure of the specimens occurred randomly within the gauge length. Figure 27 shows the progressive failure of an un-notched specimen subjected to compressive load. The initial failure is matrix cracking which can be seen as white spot on the specimen surface. The matrix cracking leads to the fiber micro-buckling, delamination and fiber breaking as the load increases, and this is further illustrated in Figure 28. Figure 28 also shows the damage zone within the specimen along the fracture plane which could be the micro-buckling of the fibers. The later stage of the damage development is a rapid increasing rate of all damage modes culminating in a critical local state of stress which initiate fracture of the specimens by shear mode. Figure 29 shows the side view of the specimen after the test and there were sign of the micro-buckling which leads to the shear failure.

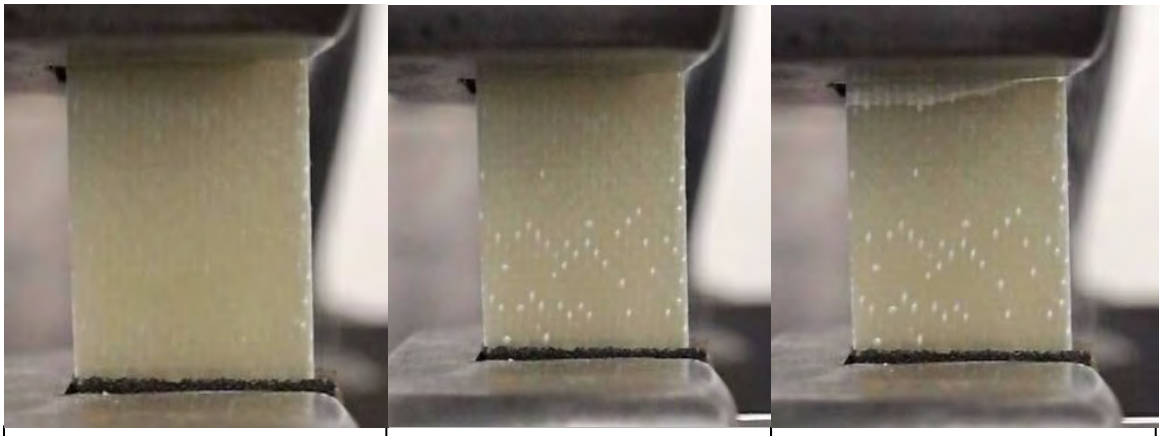

Initiation of matrix crack propagation.	Crack growth before complete fracture	Specimen fracture

Figure 27. Progressive Failure of un-notched compression specimen.

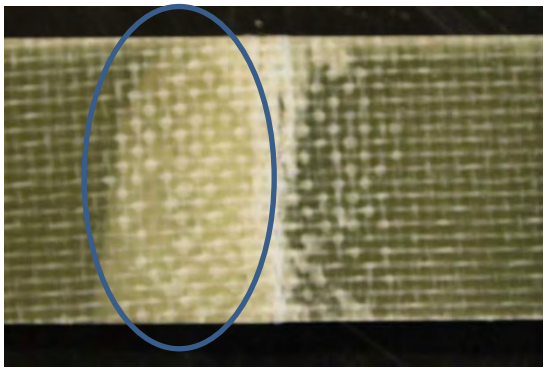

Figure 28. Post-failure observation shows signs of matrix cracking leading to micro-buckling and fiber breaking before fracture.

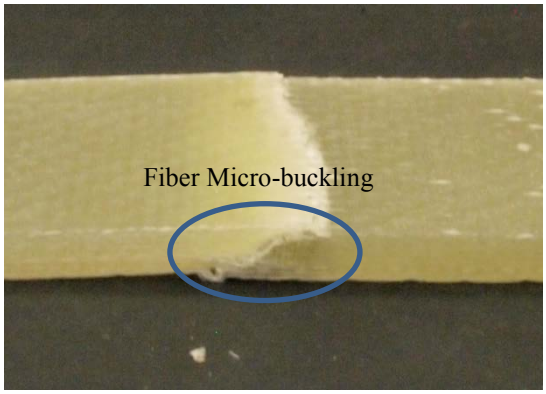

Figure 29. Post-failure observation shows specimen failure in shear mode.

The observation from the optical microscope as shown in Figure 30 and Figure 31 further enhanced the visual observation and we can see clearly that the fiber micro-buckle and break.

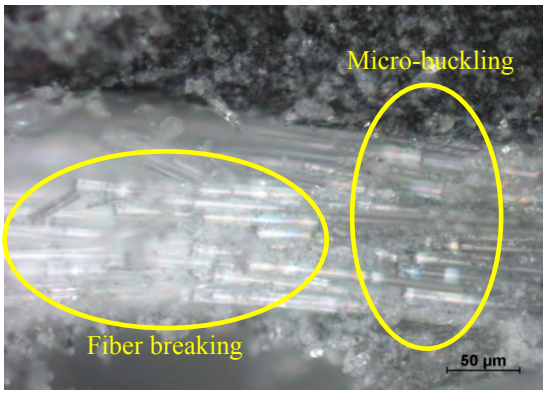

Figure 30. Post-failure observation using optical microscope shows signs of fiber micro-buckling and fiber breaking at the side of the specimen.

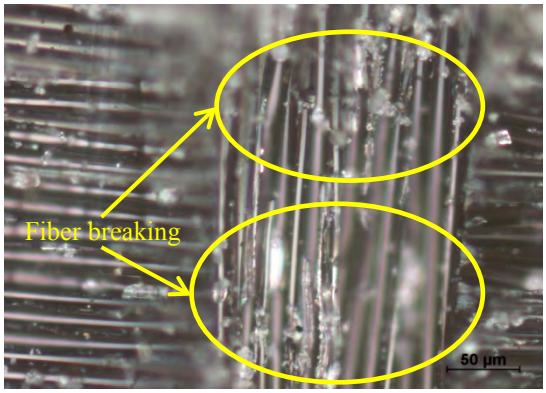

Figure 31. Post-failure observation using optical microscope shows signs of fiber breaking at the fracture edge of the specimen.

B. COMPRESSION OF PERFORATED SPECIMEN

The compressive stresses and compressive strain of the perforated specimens with different strain rates for compression test are shown in Figure 32. Although the ultimate compressive strength for the perforated specimens is lower than the un-notched

specimens for all applied strain rate, the compressive failure strain of the perforated specimens is higher than that of the un-notched specimens.

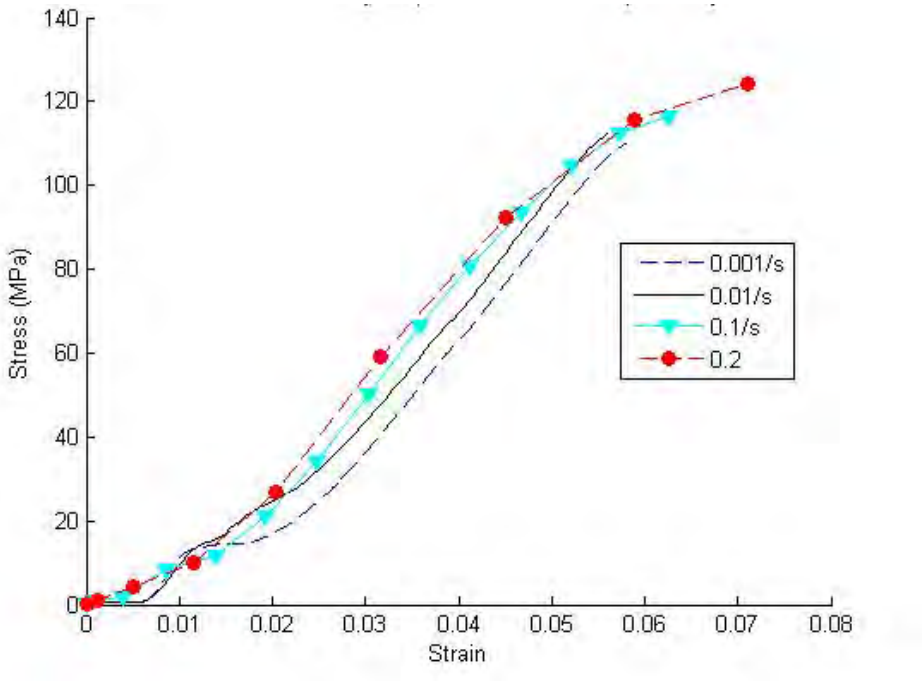

Figure 32. Compressive Stress and Strain Relationship for Perforated Specimens.

The following is a discussion of the visual observation during the tests and the inspection of the specimens after the experiment visually and using an optical microscope. In all cases, damage was not noted until at least 80% of the failure load was reached.

All the perforated compression specimens failed from the hole in a traverse direction to the loading axis at a lower stress than the un-notched compression specimens. Figure 33 shows the progressive failure of a perforated specimen subjected to compressive load. As the load increases, there was compressive stress concentration around the hole. Similar to the un-notched specimen, the perforated specimens have matrix cracking initially and micro-buckling along the plane of fracture. Subsequently, fiber micro-buckling surrounded by delamination develop at the edge of the hole at the areas of high stress concentration. This can be observed from Figure 33 which shows the longitudinal cracking extends to the left and right of the hole. As the load increases

further, the cracks extend. Failure occurs shortly thereafter, which the damage zone propagates rapidly and with a sudden and complete loss of load bearing ability. The final fracture surface is traverse to the loading axis.

Initiation of matrix crack propagation.	Crack growth before complete fracture	Specimen fracture

Figure 33. Progressive Failure of perforated compression specimen.

Figure 34 shows the damage zone within the specimen along the fracture plane which could be the micro-buckling of the fibers. As the strain rate increases, the area of the damage zone also increases. The failure in shear mode of the perforated compression specimen is similar to the un-notched specimen but it initiated from the edge of hole which can be observed from Figure 35. The observation from the optical microscope as shown in Figure 36 and Figure 37 further enhanced the visual observation.

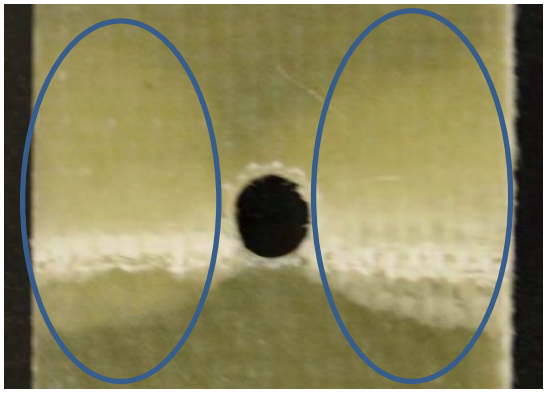

Figure 34. Post-failure observation shows signs of matrix cracking leading to micro-buckling and fiber breaking before fracture of the perforated specimen.

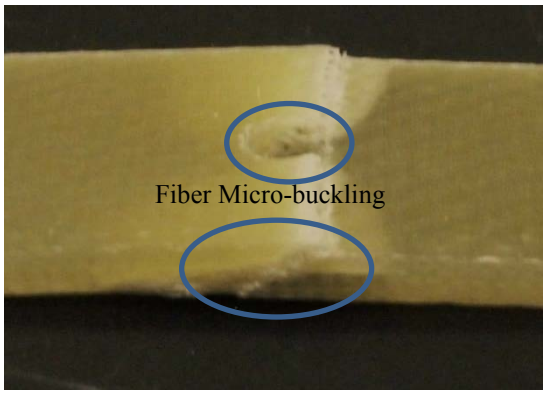

Figure 35. Post-failure observation shows failure in shear mode of the perforated compression specimen.

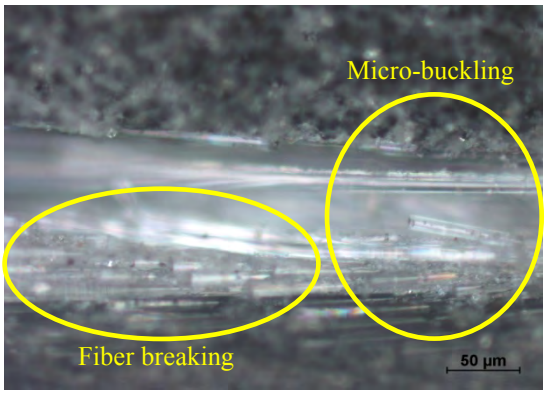

Figure 36. Post-failure observation using optical microscope shows signs of fiber micro-buckling and fiber breaking at the side of the specimen.

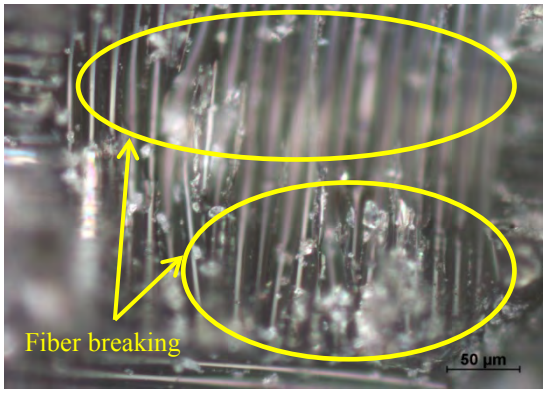

Figure 37. Post-failure observation using optical microscope shows signs of fiber micro-buckling and fiber breaking near the hole edge of the specimen.

For all the un-notched compression tests performed, micro-buckling was found to be the dominant failure mechanism within the range of the tested strain rates, followed by shear failure. The failure of the perforated specimen in compression is the initiation and growth of the micro-buckle from the edge of the hole.

The final fracture surface for both the un-notched and perforated specimen is traverse to the loading axis. The composite is strain rate sensitive as the stress and strain increases with the strain rate applied as shown in Figure 38 and Figure 39.

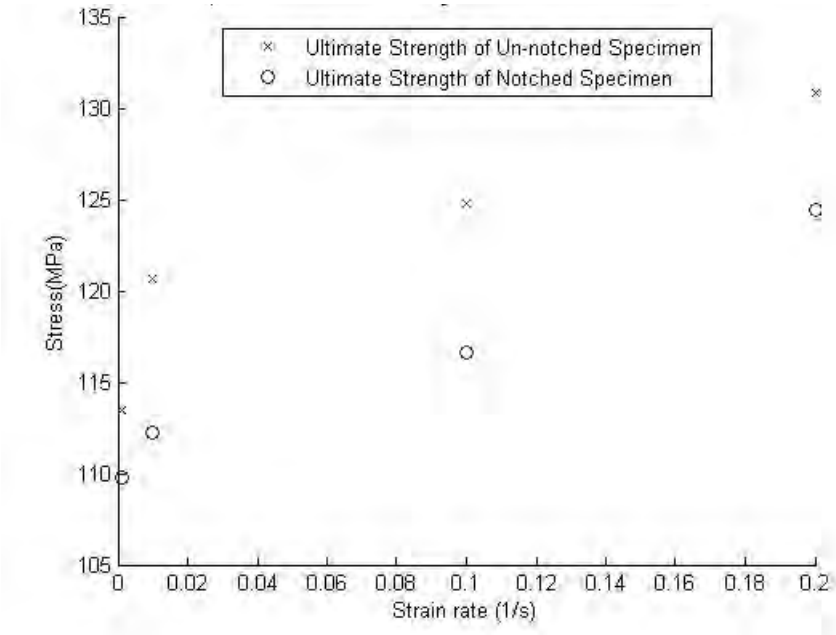

Figure 38. Comparison of the ultimate strength between perforated and un-notched specimen for compression.

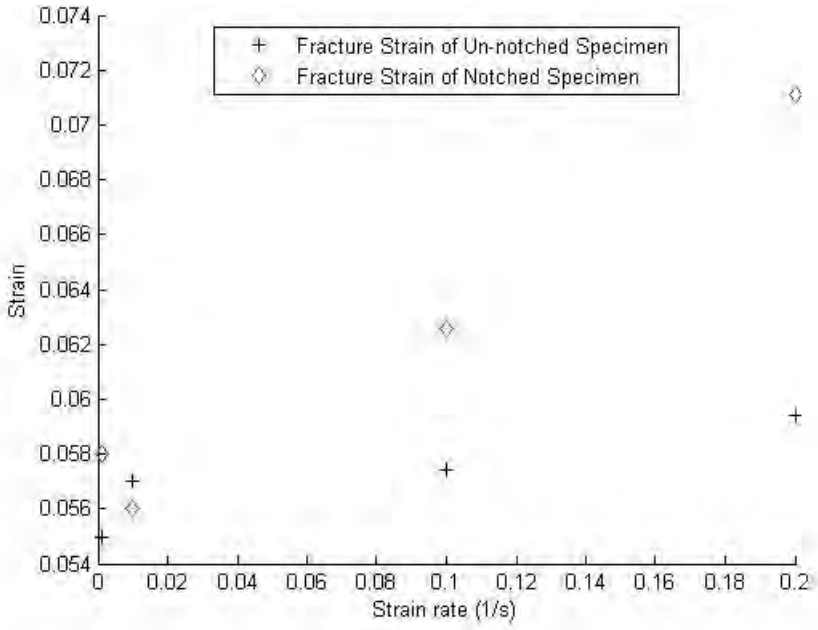

Figure 39. Comparison of the ultimate strain between perforated and un-notched specimen for compression.

C. UN-NOTCHED TENSION

The tensile stresses and strain of the un-notched specimens with different strain rate for tensile tests are shown in Figure 40. Both the tensile stress and strain increase at a higher strain rate. From analyzing the compression and tension results, we ascertained that the tensile strength is higher than the compressive strength for the present E-glass composite. We can see from the graphs that the specimen behavior is relatively consistent at different strain rate and there is no visible load drops on the curve until the specimen failure.

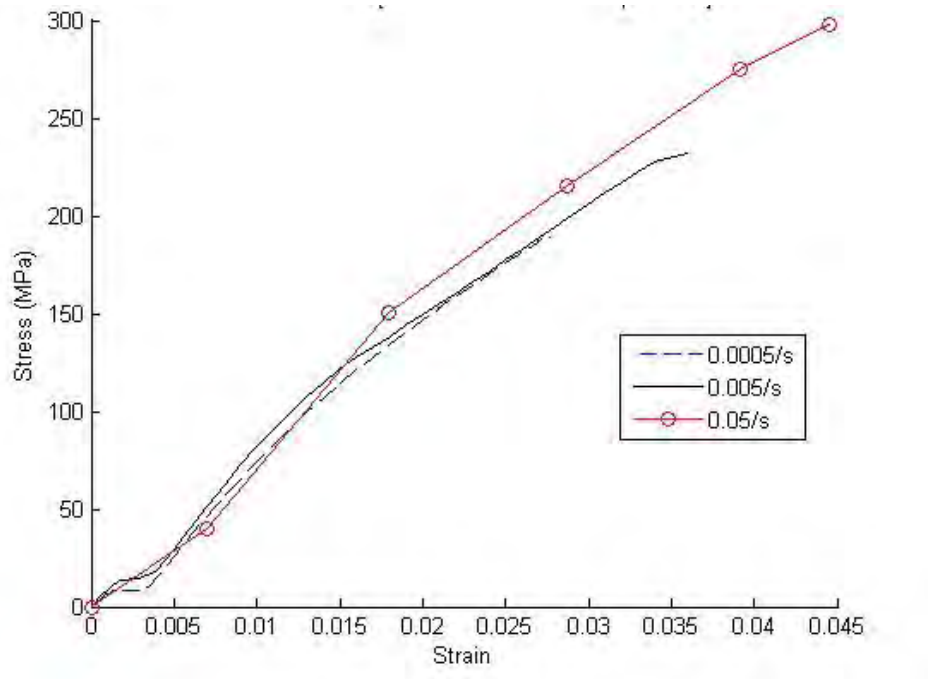

Figure 40. Tensile stress and strain relationship for un-notched specimens.

The following is a discussion of the visual observation during the tests and the inspection of the specimens after the experiment visually and using an optical microscope.

Representative images of the progressive failure of the un-notched specimens are shown in Figure 41. In general, terminal failures were consistent at different strain rate but it did not yield a clear picture of where the failure initiated. In most cases, the specimen failed within the gauge length. But there are a couple of cases where the failure occurs at the grips. In general, the specimen failure started with matrix cracking initially and it initiates from flaws in the matrix which could be the air bubbles created in the vacuum during the VARTM. Delamination and fiber breaking happens, coupled with interfacial debonding resulted in extensive matrix cracking. The later stage of the damage is a rapidly increasing rate of progression of all damage modes which fracture the specimen. “Cracking” sound was heard while testing the specimen at low strain rate which could likely depicts the last stage of the damage.

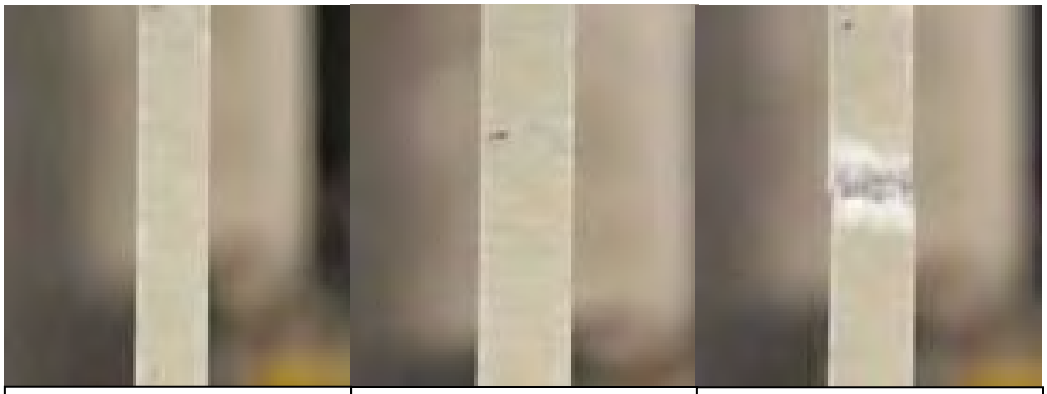

Initiation of matrix crack propagation.	Crack growth before complete fracture	Specimen fracture

Figure 41. Progressive Failure of Un-Notched Tension Specimen.

As shown in Figure 41 and Figure 42, the fracture path is fairly straight and transverse to the loading axis. Fiber breakage and matrix cracking were also observed. The observation from the optical microscope as shown in Figure 43 further enhanced the visual observation.

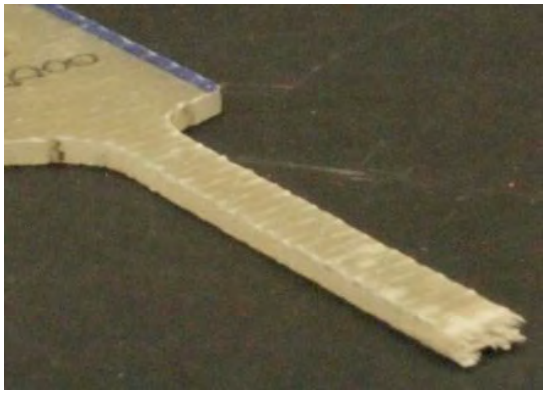

Figure 42. Post-failure observation shows signs of fiber breakage and matrix cracking at the fracture edge.

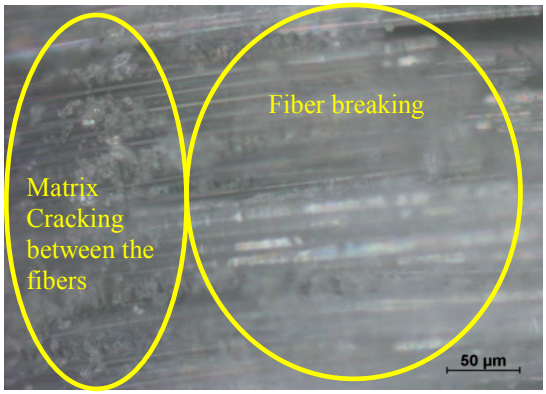

Figure 43. Post-failure observation using optical microscope shows fiber breakage and matrix cracking at the fracture edge.

D. TENSION OF PERFORATED SPECIMEN

The ultimate tensile stresses and strain of the perforated specimens with different strain rates for tensile tests are shown in Figure 44. The stress and strain increase with the increasing strain rate. By comparing Figure 40 to Figure 44, we can see that the tensile stress and strain of the un-notched specimen is higher than the perforated specimen at different strain rate. The specimen behavior was fairly consistent at different strain rates and there is no visible load drops on the curve prior to specimen failure.

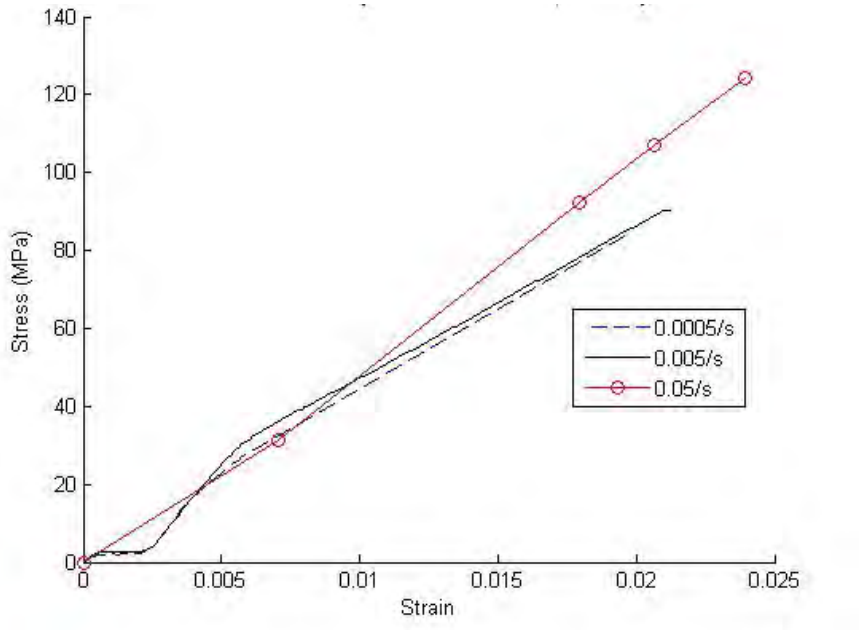

Figure 44. Tensile stress and strain relationship for perforated specimens.

The following is a discussion of the visual observation during the tests and the inspection of the specimens after the experiment visually and using an optical microscope.

The representative images of the progressive failure of the perforated specimens are shown in Figure 45. In general, all the perforated tension specimens failed from the hole in a traverse direction to the loading axis at a lower stress than the un-notched tension specimens and were consistent at different strain rates. As the load increases, the stress concentration around the hole increases, followed by delamination and fiber breaking, coupled with interfacial de-bonding resulting in extensive matrix cracking. There was also noticeable longitudinal cracking from the hole edge extending to the left and right of the hole before the terminal failure of the specimens where the fiber breaking and fiber pull out occur. A "cracking" sound was heard while testing the specimen at low strain rate which could likely depicts the last stage of the damage and the specimens snapped into two for all strain rates.

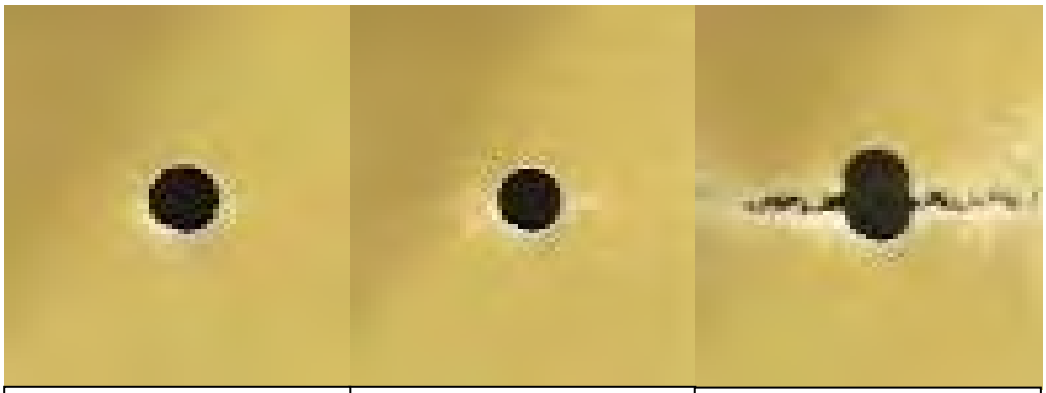

Figure 45. Progressive failure of perforated tension specimen.

As shown in Figure 46, the fracture path is fairly straight and transverse to the loading axis along the edge of the hole. Fiber breakage and matrix cracking were observed. The observation from the optical microscope as shown in Figure 47 further enhanced the visual observation.

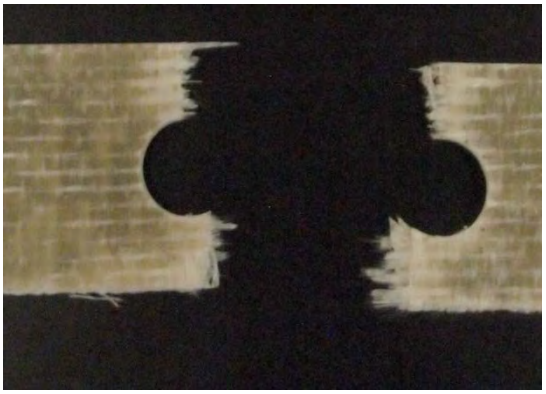

Figure 46. Post-failure observation shows signs of fiber breakage and matrix cracking along the edge of the hole.

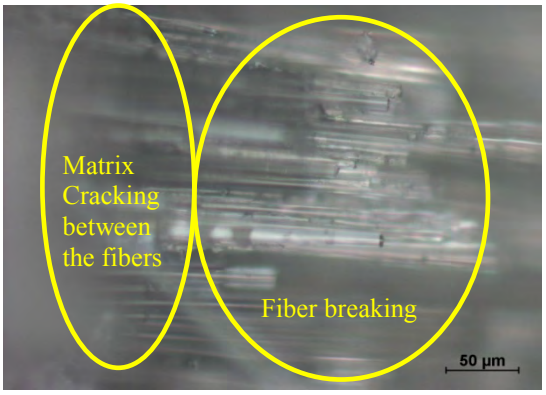

Figure 47. Post-failure observation using optical microscope shows signs of fiber breakage and matrix cracking along the edge of the hole.

For all the un-notched tension tests performed, matrix cracking and fiber breaking was found to be the dominant failure mechanism within the range of the tested strain rates. The failure of the perforated specimen in tension is similar to the un-notched specimens except that the initiation damage occurs in the form of cracking emanating from the edge of the hole due to delamination.

The final fracture surface for both the un-notched and open hole specimen is traverse to the loading axis, and failure at the hole specifically for the perforated specimen. Figure 48 and Figure 49 shows the comparison of the ultimate strength and strain between the un-notched and perforated specimen. It clearly shows that the ultimate failure strength and strain are rate dependent.

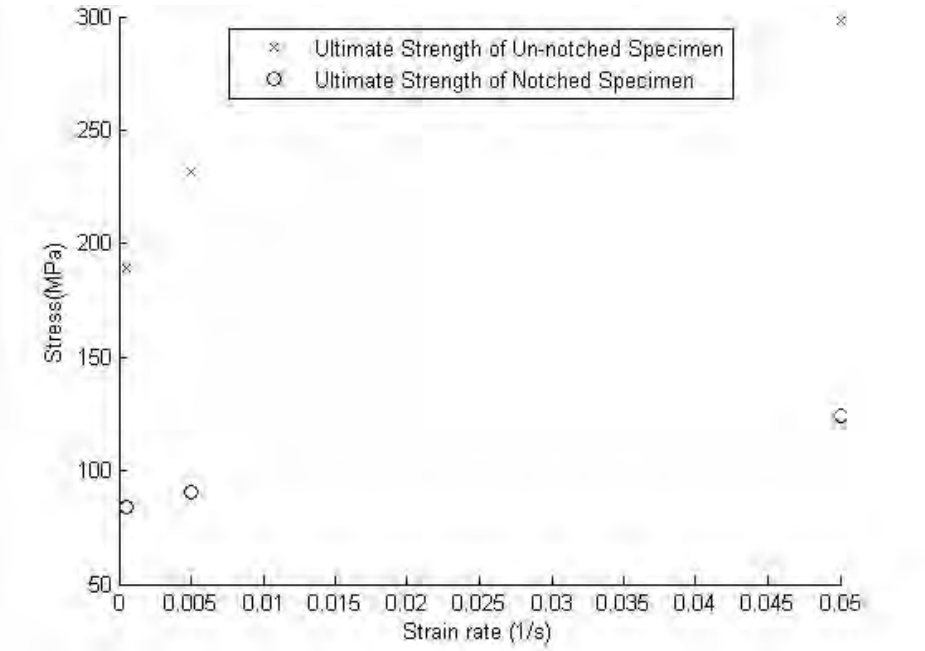

Figure 48. Comparison of the ultimate strength between perforated and un-notched specimen for tension.

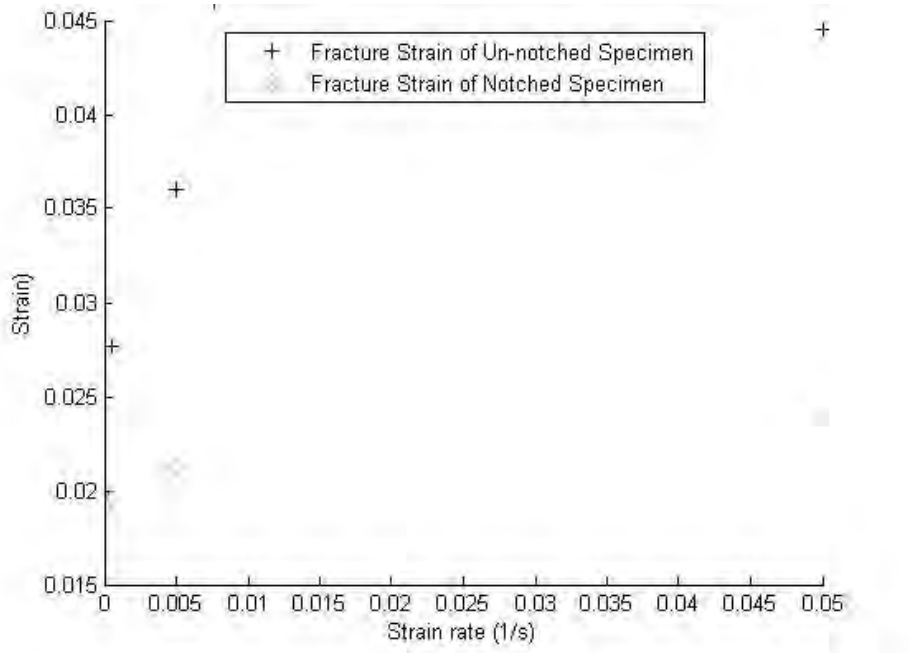

Figure 49. Comparison of the ultimate strain between perforated and un-notched specimen for tension.

E. VARYING STRAIN RATE FOR COMPRESSION AND TENSION

This section discussed the results from the varying strain rate for the un-notched specimen and perforated specimen under compression and tension loading. The fracture strength and strain of composites were varied depending on the applied strain rate loading. The strain rate was changed halfway from the first rate to the second rate and kept constant until the specimen failed.

1. Un-Notched and Perforated Compression

The results from the varying strain for the un-notched and perforated specimen under compression loading were represented in the Stress-Strain relationship plots in Figure 50 and Figure 51, respectively. They also compared the results with the highest and lowest applied constant strain rate plots.

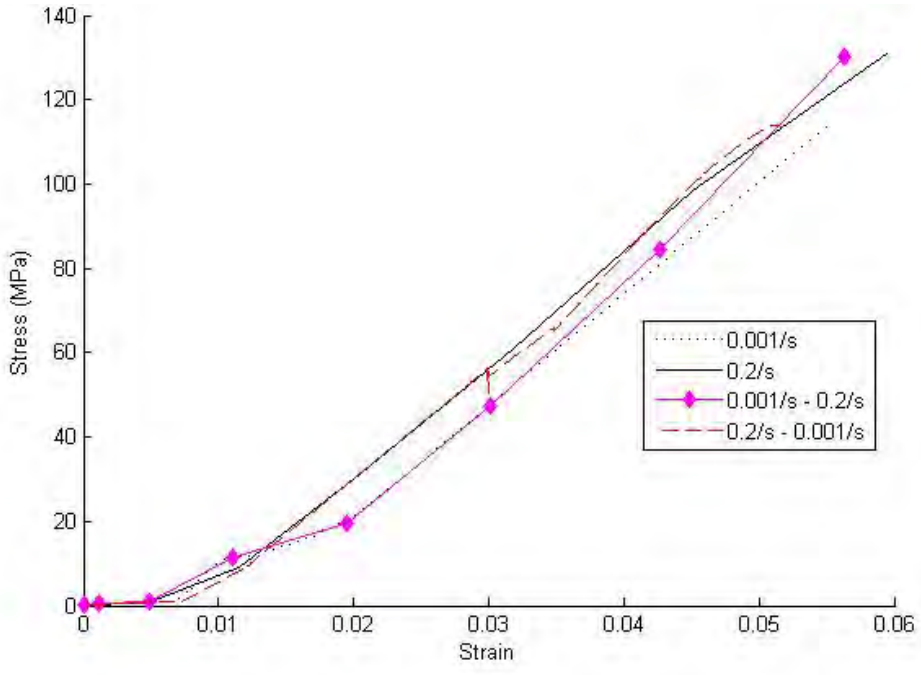

Figure 50. Comparison of varying with constant strain rate – compression, un-notched specimen.

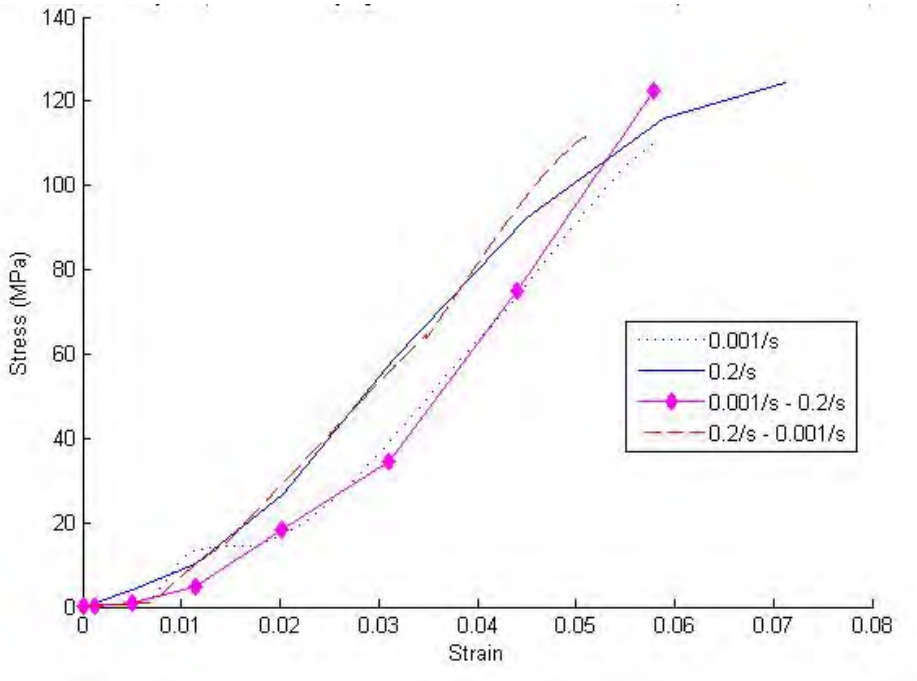

Figure 51. Comparison of varying with constant strain rate – compression, perforated specimen.

For both the figures, it is noticeable that the stress-strain curve follows that of the first uniform strain rate before the transition strain. When the strain rate was changed halfway from the first rate to the second rate, the failure strength was relatively close to that at the constant second strain rate. However, fracture strain was lower than the second strain rate.

Upon visual and optical microscope inspection, the progressive and final failure was identical to what is discussed in Section A and B of this chapter.

2. Un-Notched and Perforated Tension

The results from the varying strain for the un-notched and perforated specimen under tensile loading were represented in the Stress-Strain relationship plots in Figure 52 and Figure 53, respectively. They also compared the results with the highest and lowest applied constant strain rate plots.

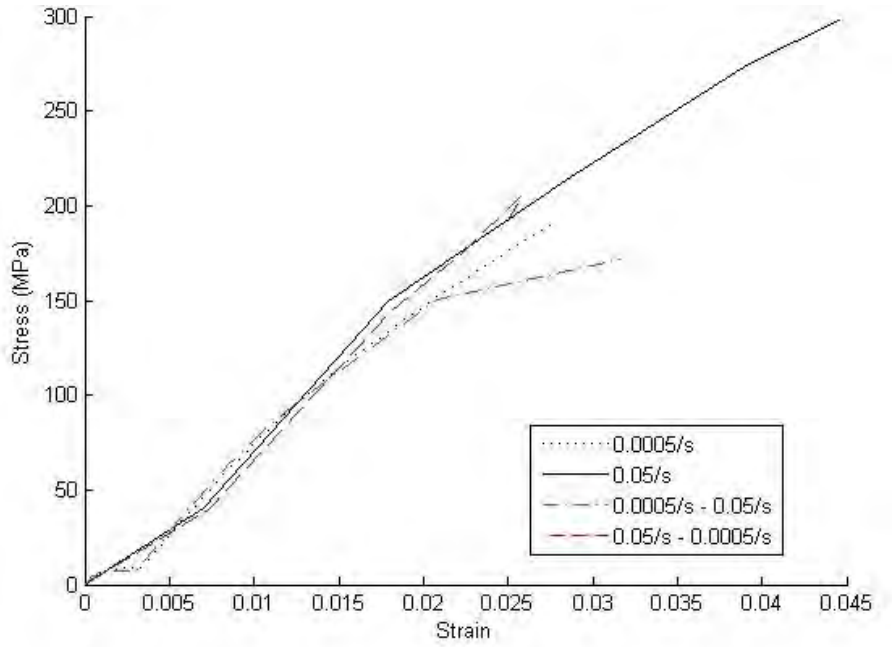

Figure 52. Comparison of varying with constant strain rate – tension, un-notched specimen.

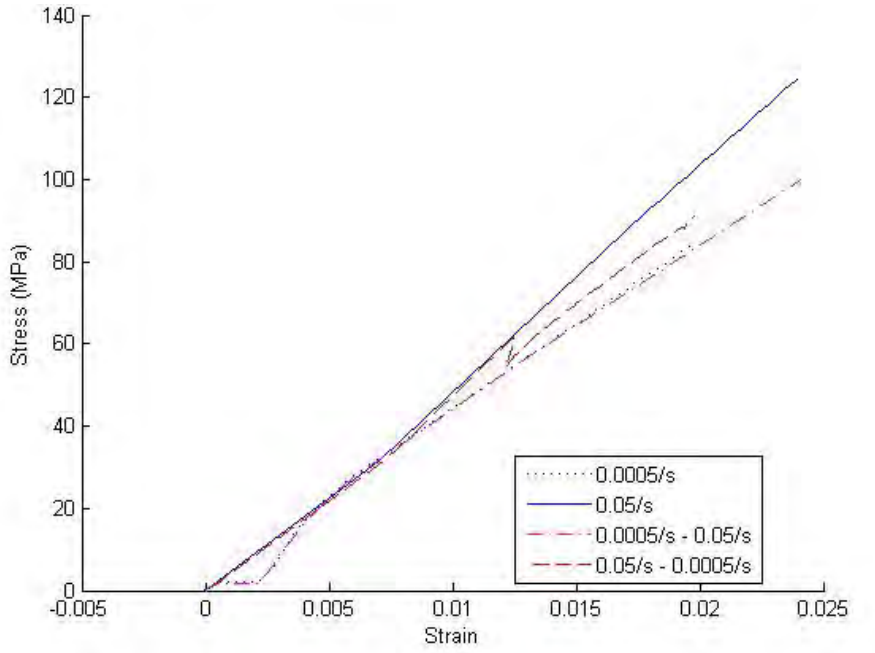

Figure 53. Comparison of varying with constant strain rate – tension, perforated specimen.

For both the figures, it is noticeable that the stress-strain curve follows that of first constant strain rate before the transition strain. Thereafter, the trend differs for the un-notched and perforated specimens.

As the un-notched tension specimens only have a thickness of 2mm and width of 5mm which were thin and slender, it was observed that the specimens almost immediately snapped into two when the strain rate transited. This caused the ultimate strength and strain to be noticeably lower than the constant strain rate plots.

As for varying strain for the perforated specimen under tension loading, the trend after the transition to the second strain rate follows the behavior of the second applied strain rate which resulted in a comparatively similar failure strain. But the ultimate tensile strength is lower than second applied strain rate.

Upon visual and optical microscope inspection, the progressive and final failure is identical to what is discussed in Section C and D of this chapter.

F COMPARISON OF ANALYTICAL STRENGTH PREDICTION WITH EXPERIMENTAL RESULTS

As discussed in Chapter II, notched strength prediction is an active area of research within the composites community and failure theories have been studied widely. Some of the theories give reasonable predictions and are easy to implement, thus the Whitney-Nuismer failure theory was implemented via the Point Stress and Average Stress Criterion for this study.

Both the un-notched and perforated strength of the laminates are known from this study, and through the video recorded for all the experiments performed, the characteristic lengths, a_o/d_o can also be approximated with reference to Figure 2 and 3. Figure 54 demonstrated the approximation of characteristic length a_o/d_o and the results are tabulated in Table 6 for the strain rate of $0.05s^{-1}$ to $0.0005s^{-1}$.

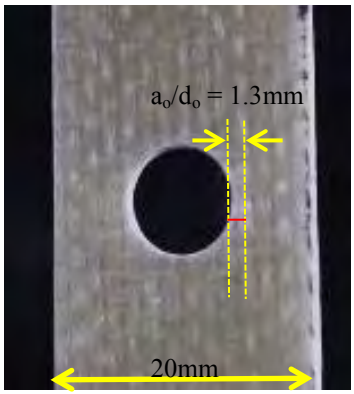

Figure 54. Approximation of characteristic length, a_o/d_o.

Table 6. Determination of the characteristic length, a_o/d_o.

	Picture		Actual	
Strain rate (s^{-1})	Length of Specimen (mm)	a_o/d_o (mm)	Length of Specimen (mm)	a_o/d_o (mm)
0.0005	45	3	20	1.3
0.005	52	2.5	20	0.96
0.05	72	3	20	0.83

The stress concentration factor for isotropic or quasi-isotopic material can be assumed to be 3 for a small hole in a large plate but in this study, the stress concentration factor used is 2.25 for the given ratio of hole radius to the specimen width [30].

By using Equation (25) to (28), the $\sigma_N^{\infty}/\ \sigma_o$ of Point Stress and Average Stress Criterion can be calculated. The results are compared with the experimental results for different strain rate and are tabulated in Table 7.

Table 7. Comparison of perforated strength between experimental and whitney-nuismer failure predication theory.

Strain rate (s^{-1})	R (mm)	K_T^{∞}	a_o/d_o (mm)	$\frac{\sigma_N^{\infty}}{\sigma_o}(Exp)$	$\frac{\sigma_N^{\infty}}{\sigma_o}(PSC)$	% Error	$\frac{\sigma_N^{\infty}}{\sigma_o}(ASC)$	% Error
0.0005	4	2.25	1.3	0.442	0.543	18.5	0.468	5.6
0.005	4	2.25	0.96	0.390	0.498	21.7	0.453	13.8
0.05	4	2.25	0.83	0.417	0.482	13.4	0.447	6.75

From Table 7, the Average Stress Criterion predicted relatively closer to the experimental results compared to the Point Stress Criterion. The Point Stress and Average Stress Criterion only utilize the stress concentration factor to determine the stress distribution in the laminate, and because the stress concentration factor does not vary from different strain rate, no large change is predicted. But the experimental results show otherwise. The ultimate strain and stress increases as the strain rate increases, although the characteristics length reduces. Thus, there is strain rate effect on the stress concentration at the hole and that should differ when under different strain rate loading. The stress concentration factor considered is for a homogenous specimen. However, composite laminate is not homogenous and the stress concentration of the open hole largely depends on the matrix cracking at the edge of the hole. Hence, it is apparent that the Whitney-Nuismer failure theory considered here are not sensitive enough to consider for different strain rate.

THIS PAGE INTENTIONALLY LEFT BLANK

IV. CONCLUSION AND RECOMMENDATIONS

In conclusion, the composite is strain rate sensitive as the stress and strain increases with the strain rate applied. Although the ultimate compressive strengths for the perforated specimens are lower than those of the un-notched specimens for all applied strain rates, the compressive fracture strains of the perforated specimens are consistently higher than those of the un-notched specimens. When the specimens were subjected to tension loads, the tensile strength and fracture strain of the un-notched specimen is higher than the perforated specimen at different strain rates.

For the non-uniform varying strain rate during compression test, it was noticeable that the stress-strain curve during the first strain rate followed that of the constant strain rate before the transition strain. When the strain rate was changed halfway from the first rate to the second rate, the failure strength was relatively close to that at the constant second strain rate. However, the fracture strain was lower than that at the second strain rate.

Similar to the compression test, the stress-strain graph during the first strain rate followed that of the constant strain rate before the transition strain for the varying strain rate tension test. Thereafter, the trend differed for the un-notched and perforated specimens. The perforated specimen under varying strain rate failed almost at the same fracture strains of the second strain rate while their tensile strength were between those of respective constant strain rates. For the un-notched specimens, either the tensile strength or the fracture strain under a varying strain rate was smaller than that of any respective constant strain rate. If the strength for the varying strain rate was the smallest, the associated fracture strain was bounded between the two values of respective constant strain rates. This was also true as far as the fracture strain was concerned.

Whitney-Nuismer failure theory, namely the Point Stress and Average Stress Criterion was implemented as it gave reasonable prediction and easy to implement. But after implementation, it was apparent that the Whitney-Nuismer failure theory considered here was not sensitive enough to consider for different strain rates.

There are several aspects where the current work can be extended.

i) X-ray radiography can be used to during the test and after the test to give additional insights into the progressive damage characteristics of the composite material.

ii) The range of strain rates used for the varying strain rate compression and tension test may be increased to have a more distinct resolution of the stress and strain relationship and behavior of the composite material.

iii) Different sizes of circular open hole with different uniform and non-uniform strain rate may be investigated and tested. By studying the results, the hole size and stress concentration at the hole for different strain rate can be established and compared.

iv) An extensive amount of testing has been done for compression and tension for open hole and un-notched composite in this study. But most applications are multi-axial so that multi-axial testing may be further explored and investigated.

v) There is no reliable failure criterion for varying strain rate loading currently. Thus, it will be beneficial to have one proposed although complex finite element analysis and substantial computational effort will be required.

LIST OF REFERENCES

[1] N. Taniguchi, T. Nishiwaki, N. Hirayama, H. Nishida, and H. Kawada, "Dynamic tensile properties of carbon fiber composite based on thermoplastic epoxy resin loaded in matrix-dominated directions," *Composites Science and Technology*, vol. 69, pp. 207–213, Feb 2009.

[2] O. I. Okoli, and G. F. Smith, "The effect of strain rate and fibre content on the Poisson's ratio of glass/epoxy composites," *Composite Structures*, vol. 48, pp. 157–161, Jan 2000.

[3] M. M. Shokrieh, and M. J. Omidi, "Tension behaviour of unidirectional glass/epoxy composites under different strain rates," *Composite Structures*, vol. 88, pp. 595–601, Mar 2009.

[4] R. O. Ochola, K. Marcus , G. N. Nurick , and T. Franz, "Mechanical behaviour of glass and carbon fibre reinforced composites at varying strain rates," *Composite Structures,* vol. 63, pp. 455–467, Mar 2004.

[5] J. L. Tsai, and C. T. Sun, "Dynamic compressive strengths of polymeric composites," *International Journal of Solids and Structures*, vol. 41, pp. 3211 – 3224, Jun 2004.

[6] J. Backlund and Carl-Gustaf Aronsson, "Tensile Fracture of Laminates with Holes," *Journal of Composite Materials*, vol. 20, pp. 259–286, May 1986.

[7] I. Eriksson, and Carl-Gustaf Aronsson, "Strength of Tensile Loaded Graphite/Epoxy Laminates containing Cracks, Open and Filled holes," *Journal of Composite Materials*, vol. 24, pp. 456–482, May 1990.

[8] Jung-Kyu Kim, Do-Sik Kim, and N. Takeda, "Notched Strength and Fracture Criterion in fabric composite plates containing a Circular Hole," *Journal of Composite Materials*, vol. 29, pp. 982–998, May 1995.

[9] C. Soutis, and N. A. Fleck, "Static Compression Failure of Carbon Fibre T800/924C Composite with a Single Hole," *Journal of Composite Materials*, vol. 24, pp. 536–558, May 1990.

[10] E. G. Guynn, W. L. Bradley, and W. Elber, "Micromechanics of Compression Failures in open Hole Composite Laminates," *Composite Material: Fatigue and Structure*, vol. 2, ASTM STP 1012, pp. 118–136, 1989.

[11] P. K. Gotsis, C. C. Chamis and L. Minnetyan, "Prediction of Composite Laminate Fracture: micromechanics and progressive fracture," *Computer Science and Technology*, vol. 58, pp. 1137–1149, Jul 1998.

[12] M. J. Hinton, A. S. Kaddour, and P. D. Soden, "A further assessment of the predictive capabilities of current failure theories for composite laminates: comparison with experimental evidence," *Composites Science and Technology*, vol. 64, pp. 549–588, Mar 2004.

[13] M. E. Waddoups, "Characterization and design of composite materials," *Composite Materials Workshop*, S. W. Tsai, J. C. Halpin, and N. J. Pagano, Ed. Lancaster: Technomic Pub. Co, pp. 254–308, 1968.

[14] Stephen W. Tsai and Edward M. Wu," A General Theory of Strength for Anisotropic Materials," *Journal of Composite Materials*, vol. 5, pp. 58–80, Jan 1971.

[15] Z. Hashin, "Failure Criteria for Unidirectional Fiber Composites," *Journal of Applied Mechanics*, vol. 47, pp. 329–334, Jun 1980.

[16] M. E. Waddoups, J. R. Eisenmann and B. E. Kaminski, "Macroscopic Fracture Mechanics of Advanced Composite Materials," *Journal of Composite Materials*, vol. 5, pp. 446–454, Oct 1971.

[17] E. Wu, "Fracture Mechanics of Anisotropic Plates," *Composite Materials Workshop*, S. W. Tsai, J. C. Halpin, and N. J. Pagano, Ed. Lancaster: Technomic Pub. Co, pp. 20–43, 1968.

[18] G. R. Irwin, "Fracture Dynamics," *Fracture of Metals*, ASM, 1948.

[19] O. L. Bowie, "Analysis of an Infinite Plate Containing Radial Cracks Originating from the Boundary of an Internal Hole," *Journal of Mathematics and Physics*, pp. 60–71, 1956.

[20] P. C. Paris, and G. C. Sih, "Stress Analysis of Cracks," *Fracture Toughness Testing and its Applications*, ASTM STP 381. pp. 30–85. Apr 1965.

[21] J. M. Whitney and R. J. Nuismer, "Stress Fracture Criteria for Laminated Composites Containing Stress Concentrations," *Journal of Composite Materials*, vol. 8, pp. 253–265, Jul 1974.

[22] J. Awerbuch and M. S. Madhukar, "Notched Strength of Composite Laminates: Predictions and Experiments- A Review," *Journal of Reinforced Plastics and Composites*, vol. 4, pp. 3–159, Jan 1985.

[23] S. P. Timoshenko and J. N. Goodier, *Theory of Elasticity* (2nd ed.). New York: McGraw-Hill, 1951.

[24] H. J. Konish and J. M. Whitney, "Approximate Stresses in an Orthotropic Plate Containing a Circular Hole," *Journal of Composite Materials*, vol. 9, pp. 157–166, Apr 1975.

[25] S. G. Lekhnitskii, *Anisotropic Plates* (2nd ed.). New York: Gordon and Breach, Science Publishers Inc., 1968.

[26] J. Backlund, "Fracture Analysis of Notched Composites." *Computers and Structures*, vol. 13, pp. 145–154, 1980.

[27] A. Hillerborg, M. Modeer, and P. E. Petersson, "Analysis of Crack Formation and Crack Growth in Concrete by Means of Fracture Mechanics and Finite Elements," *Cement and Concrete Research*, vol. 6, pp. 773–782, Aug 1976.

[28] C. Soutis and P. T. Curtis, "A method for predicting the fracture toughness of CFRP laminates failing by fibre microbuckling," *Composites Part A: Applied Science and Manufacturing*, vol. 31, pp. 733–740, Jul 2000.

[29] J. E. Klopfer, "An experimental study of fiberglass composite containing metal Wire Joints" M.S. thesis, Naval Postgraduate School, 2009.

[30] A. C. Ugural and S. K. Fenster, *Advanced Strength and Applied Elasticity* (4th ed.). New Jersery: Prentice Hall, 2003.

THIS PAGE INTENTIONALLY LEFT BLANK

INITIAL DISTRIBUTION LIST

1. Defense Technical Information Center
   Ft. Belvoir, Virginia

2. Dudley Knox Library
   Naval Postgraduate School
   Monterey, California

3. Young W. Kwon
   Naval Postgraduate School
   Monterey, California

4. Jarema M. Didoszak
   Naval Postgraduate School
   Monterey, California

5. Yew Khuan Boey
   Singapore Technologies Kinetics
   Singapore

6. Tat Soon Yeo
   Temasek Defence Systems Institute, National University of Singapore
   Singapore

7. Lai Poh Tan
   Temasek Defence Systems Institute, National University of Singapore
   Singapore